CZECH TECHNICAL UNIVERSITY IN
PRAGUE

Faculty of Nuclear Sciences and Physical
Engineering

Department of Physics

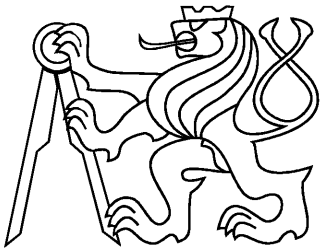

Research Project

t-Dependence of the cross section for the coherent production of J/ψ in Pb-Pb UPC

Bc. Roman Lavička

Supervisor: prof. Jesús Guillermo Contreras Nuño, Ph.D.

Prague, 2015

ČESKÉ VYSOKÉ UČENÍ TECHNICKÉ V PRAZE
FAKULTA JADERNÁ A FYZIKÁLNĚ INŽENÝRSKÁ
PRAHA 1 - STARÉ MĚSTO, BŘEHOVÁ 7 - PSČ 115 19

Katedra: fyziky **Akademický rok:** 2014/2015

VÝZKUMNÝ ÚKOL

Posluchač: Bc. Roman Lavička

Obor: Experimentální jaderná a částicová fyzika

Vedoucí úkolu: prof. Guillermo Contreras Nuno, Ph.D., FJFI ČVUT

Název úkolu (česky/anglicky):
Závislost účinného průřezu na přenesené čtyřhybnosti t^2 pro koherentní produkci J/Psi v Pb-Pb UPC
t-Dependence of the cross section for the coherent production of J/Psi in Pb-Pb UPC

Pokyny pro vypracování:

1. Použití MC simulací rozpadu J/Psi na 2 miony ke studiu změny přenesené čtyřhybnosti t^2 pro definování vhodných intervalů měření, vyvažováním hraniční statistiky s použitím několika intervalů v t^2.
2. Rozhodnutí, jestli rozdělení do intervalů je vhodné nebo je třeba provést „unfolding". K tomu rozhodnout, jestli je popis pomocí MC dostatečný nebo je třeba ho přenastavit.
3. Použití MC simulací nekoherentní produkce ke studiu pozadí a jeho vlivu na předchozí výsledky.
4. Použití MC simulací koherentní produkce Psi(2S) ke studiu vlivu „feed-down".
5. Získání předběžného účinného průřezu na přenesené čtyřhybnosti t^2 pro koherentní produkci J/Psi v Pb-Pb UPC pro střední rapiditu dat nabraných na experimentu ALICE v roce 2011.

Práce bude vypracována v anglickém jazyce.

Součástí zadání výzkumného úkolu je jeho uložení na webové stránky katedry fyziky.

Literatura:

[1] B. Abelev et al. [ALICE Collaboration], Charmonium photoproduction at midrapidity in ultra-peripheral Pb-Pb collisions at $\sqrt{s_{NN}} = 2.76$ TeV, arXiv:1305.1467 [nucl-ex]

[2] The ALICE experiment at the CERN LHC, ALICE Collaboration (K. Aamodt (Oslo U.) et al.). 2008. 259 pp., Published in JINST 3 (2008) S08002

[3] ALICE internal notes

Datum zadání: 16.10.2014 .....

Datum odevzdání: 26.06.2015 ***Vedoucí katedry***

Prohlášení:

Prohlašuji, že jsem svůj výzkumný úkol vypracoval samostatně a použil jsem pouze podklady (literaturu, software, atd.) uvedené v přiloženém seznamu.

Nemám závažný důvod proti užití tohoto školního díla ve smyslu 60 Zákona .121/2000 Sb., o právu autorském, o právech souvisejících s právem autorským a o změně některých zákonů (autorský zákon).

V Praze dne 26. června 2015

Roman Lavička

Title:
t-Dependence of the cross section for the coherent production of J/Ψ in Pb-Pb UPC

Author: Roman Lavička

Specialization: Experimental nuclear and particle physics

Sort of project: Research project

Supervisor: prof. Jesús Guillermo Contreras Nuño, Ph.D.

Abstract:
Several models were created for a computation of the parton distribution function and their predictions for small Bjorken x awaiting an experimental confirmation. Solutions of this function can be experimentally obtained from a measurement of a cross section. We focus on an ultra-peripheral collision of lead-lead nuclei producing a J/Ψ meson. Our main task is to calculate a t-dependence of the cross section. In this report we publish our results of calculations of the acceptance and the efficiency of the detector ALICE for measured process, decision of the best binning order for our data and results of the fits of the Monte Carlo coherent data.

Key words: Ultra-peripheral heavy-ion collisions, ALICE, J/Ψ, electromagnetic interaction, cross section

Název práce:
Závislost účinného průřezu na přenesené čtyřhybnosti t^2 pro koherentní produkci J/Ψ v Pb-Pb UPC

Autor: Roman Lavička

Abstrakt:
Za účelem vypočítání partonové distribuční funkce bylo vytvořeno několik modelů a jejich předpovědi pro malá Bjorkenova x čekají na experimentální ověření. Řešení této rovnice lze experimentálně získat z měření účinného průřezu. My se zaměřujeme na ultraperiferální srážky jader olova, které produkují J/Ψ mezon. Naším hlavním úkolem je spočítat závislost účinného průřezu na t. V této stati publikujeme naše výsledky výpočtů akceptance a efektivnosti detektoru ALICE pro náš proces, rozhodnutí o nejlepším rozdělení intervalů pro naše naměřená data a výsledky fitů z Monte Carlo koherentních dat.

Klíčová slova: ultraperiferální srážky těžkých iontů, ALICE, J/Ψ, elektromagnetická interakce, účinný průřez

Acknowledgement

I would like to express my gratitude to my supervisor prof. Jesús Guillermo Contreras Nuño, Ph.D. for his invaluable advice, support and language and factual corrections during this work. I would also like to express my gratitude to my CERN Summer Student Programme supervisor Dr. Evgeny Kryshen for the opportunity to spend an amazing summer side-by-side the best people in the field and gaining new knowledge. I would also like to thank to Mgr. Michal Broz, Ph.D for his preparation of the Monte Carlo simulations and to Ing. Jaroslav Adam for his quick helps with programming difficulties.

Preface

One of the main goals of physics is to give an answer to a question - what are we made of? As technology improves we got an ability to study smaller and smaller pieces of our world, revealing that matter is made of atoms, atoms are made of their nuclei and electrons and so on. Nowadays modern detectors gives us an opportunity to measure the distribution of quarks and gluons inside hadrons. This report should give us a better understanding of data taken at LHC facility during ultra-peripheral lead-lead collisions in 2011 and help us to prepare a new measurement with the data to be taken at the end of 2015.

In this report we focus on events, where only one J/ψ meson was created in the collision of lead ions and decayed to a muon pair. Our main interest is to calculate cross section dependence of such process on transferred momentum t, when the J/ψ was created at mid-rapidity. Data have been already analysed by ALICE and cross section dependence on rapidity y was calculated [1]. Results were compared to several models and came up with that only those with mild shadowing could successfully described the measure data. The dependence of cross section on t maps the gluon distribution on the impact parameter plane. Its measurement will help to constraint even more the models and will yield a new understanding of the gluon distribution in lead nuclei.

A brief look at a physics relevant for this measurement is mentioned in Chapter 1 - Introduction. In the next chapter, which is focused on theory, we explain, what are ultra-peripheral collisions, the J/ψ particle, kinematic variables used and how we calculate the cross section. Because a lot of work was done to analyse the data, we describe them and the whole work-flow in the Chapter 3. The results with discussion are summed up in the Chapter 4. In Chapter 5 we described the work on a tool to compute the luminosity. This tool is of utility to the whole Collaboration and in particular, will be useful to compute the luminosity for the measurement we are interested in. The last chapter contains a summary.

Contents

List of Figures

List of Tables

Chapter 1

Introduction

1.1 Small-x physics

Parton distribution function (PDF) describes a distribution of quarks and gluons (partons) in matter. Before turning on the LHC facility in 2009 the proton PDF was well known for so-called Bjorken x and scale Q^2 as it was measured with high precision at HERA in Hamburg [2]. With LHC we got an opportunity to study the PDF of lead nuclei at small values of x for perturbative scales Q^2 and thus, one could be more sensitive to saturation effects if they are present at LHC energies.

1.1.1 Fraction of momentum

In infinite momentum frame the Bjorken x is related to a ratio of the momentum carried by gluon or quark in the nucleon (nucleus) to the total momentum of the nucleon (nucleus). A powerful tool for studying PDFs at small x is deep inelastic scattering (DIS). Here, in high energy limit, the x is related to transferred momentum via the centre-of-mass energy s as $s \sim \frac{Q^2}{x}$. In Fig. 1.1 one can see a distribution functions for quarks and gluons in a proton for a fixed Q^2.

1.1.2 Gluon distribution function

The reason, why we want to compute a dependency of the cross section for the coherent production of J/ψ on the transferred momentum t is its connection with gluon distribution function in Pb $\sigma \sim G^2(x, Q^2)$, where Q^2 is related to the mass of the J/ψ and thus it is expected to be in the perturbative regime. This distribution cannot be obtained by rescaling the gluon distribution function according to its nucleon number N and proton number Z. With increasing centre-of-mass energy we expect that there will be relatively more gluons in nucleus than in nucleon at the same energies. But for Bjorken x below 0.1 so called shadowing appears and the ratio of structure function of nucleus to structure function of proton decrease. This is an experimental fact and also results of this paper could be used to explain this behaviour. An example of a progression of this ratio is shown in Fig. 1.2

LHC provides collisions at higher energies, which gives as a better resolution in Q^2 for certain x. The rapidity of the coherently produced J/ψ is related to the Bjorken-x. At mid-rapidity the process is sensitive to x 10^{-3} for Run1 energies and x 10^{-4} for Run2 energies. The $G(x, Q^2)$

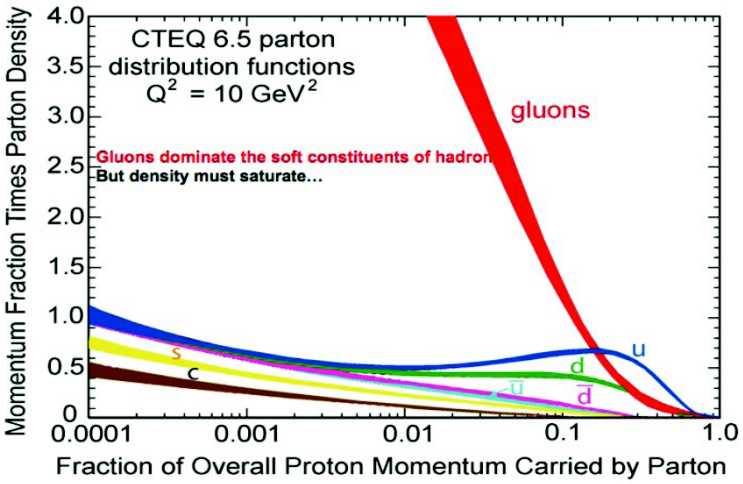

Figure 1.1: Parton distribution function for different partons.[3]

distribution does not carry information about the distribution of gluons in the plane transverse to the interaction, the so called impact-parameter plane. Saturation models predict interesting signatures in this plane. To access this information, we also need to measure the t-dependence of the cross section at a given rapidity. As it will be discussed later, a J/ψ meson with its mass is an ideal particle to study this distribution.

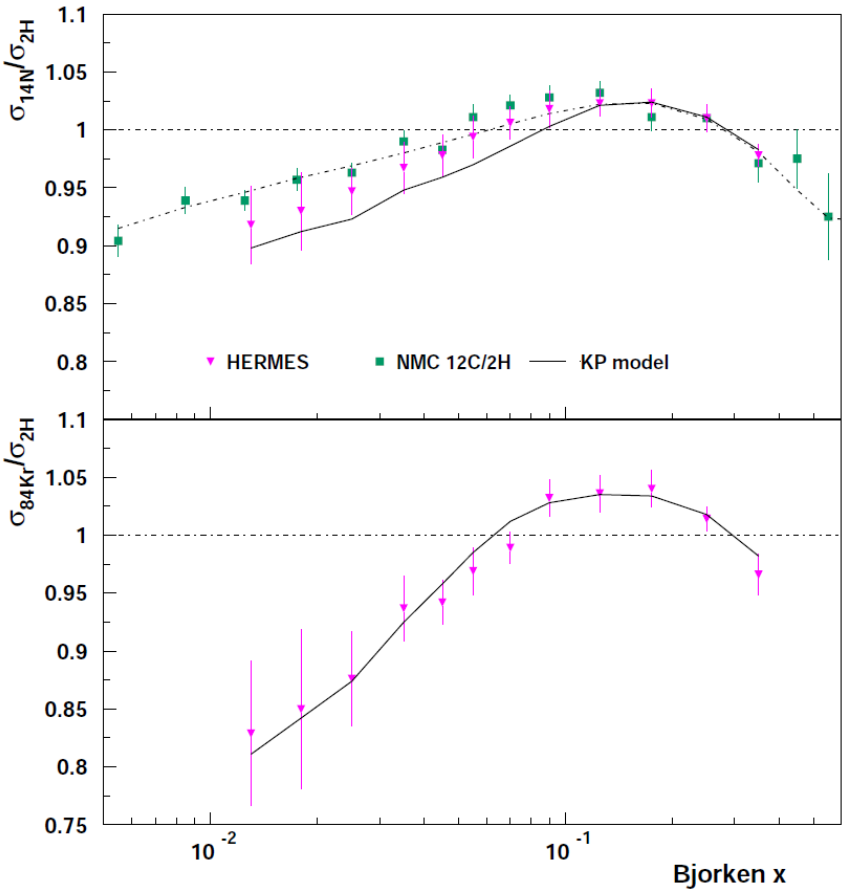

Figure 1.2: A ratio of cross sections of light nucleus and heavy nucleus. Data are obtained from the HERMES experiment (Illustrational figure).[4]

Chapter 2

Theory

2.1 Ultra-peripheral collisions

An ultra-peripheral collision (UPC) is defined as a collision, where two projectiles with radii R_A and R_B pass by with an impact parameter b larger then the sum of these radii. A sketch of such collision is shown in Fig. 2.1. Experimental high-energy physics uses projectiles with radius of few femtometers. Therefore impact parameter is larger than the range of weak and strong interactions and because the gravitational interaction is very small in comparison with other forces, UPC are mediated by electromagnetic interactions. Hence, one can imagine these collisions as an interaction of clouds of virtual photons, which surround our projectiles.

Any charged particle can be used as a projectile for UPC. But the number of surrounding photons depends on the atomic number Z, so the intensity of interaction grows with Z^2. From this condition one can see an advantage of heavy-ion collisions for UPC. Nowadays, the physics of UPC is studied at RHIC and LHC facilities using a variety of projectiles. In this report we analyse lead-lead collisions at LHC at 2.76 TeV per nucleon pair. The goal is two-fold: on the one hand to develop the tools to perform this measurement during Run2, where we will have many more events at our disposal and the events will be at very small Bjorken-x and on the other hand to evaluate if it is possible to perform this measurement, albeit with large errors, using existing Run1 data.

In general, two types of UPC can occur. One is called photon-photon collision and in this case photons from mother nuclei interact with each other. As a result new particles appear (i.e. $\mu^+\mu^-$ pairs or $q\bar{q}$ pairs). However, due to law of conservation of total angular momentum a creation of one vector meson cannot happen. For this we need more photons in the interaction or the second type of collision; photon-nucleus collision. A diagram for such process is shown in Fig. 2.2. Here we can see one nucleus, which emits the photon. This nucleus doesn't loose much energy with respect to the other nucleus. Afterwards this photon fluctuates into a virtual $q\bar{q}$ pair. This pair is a colour dipole, which interacts strongly with the second nucleus to produce a vector meson. In this work we are interested in the case of the vector meson being a J/ψ particle. The second nucleus contributes to the momentum for the created J/ψ particle. This is the transferred momentum t between the initial and final nucleus acting as target. The subject of this thesis is to evaluate the possibility of measuring the cross section of J/ψ photoproduction as a function of t at mid-rapidity using the ALICE detector.

The exclusive photoproduction of vector meson is the subject of study of this thesis. We

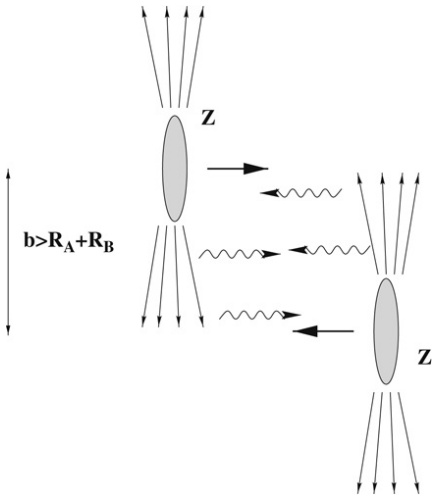

Figure 2.1: A diagram of ultra-peripheral collisions of two ions (proton number Z) with impact parameter b. Reprinted from [5].

have two types of this production. Coherent one, where the photon interacts coherently with almost all nucleons in nucleus (it couples with whole nucleus), or incoherent one, where the photon interacts with single nucleon. In our analyses we can distinguish between these two production types through the use of transverse momentum of the J/ψ, which is related to the transverse size of the target. While the coherent production is characterized with low momentum ($p_t \approx 60$ MeV/c), the incoherent one is more probable in higher momentum ($p_t \approx 500$ MeV/c) [1]. In the first case, nucleus usually doesn't break, but adding another photon interaction, we can observe such decay. The second case photoproduces J/ψ particles and brings an advantage against photoproduction in forward region; no other particles are produced.

2.2 The J/ψ particle

A J/ψ is a vector meson. Its main atributes are in Tab. 2.1. States, which are composed of $c\bar{c}$ quarks, are called charmonium and the J/ψ is related to its ground state. The whole family can be seen in Fig. 2.3. In Tab. 2.2 are decay channels of the J/ψ. We can see, that decays to hadrons are the most probable one. Probabilities of decay to dileptons are almost the same (with a little bit higher chance for e^+e^-). Unfortunately, decays to hadrons are quite complicated and it is difficult to reconstruct them. In this paper we focus only on $\mu^+\mu^-$ channel, because when muons propagates through detectors, they don't irradiate as easily as electrons do and therefore we should get a better resolution in $|t|$.

The beauty of this meson is its sharp peak, which can be found at 3.1 GeV. This we can compare with other vector mesons in the Fig. 2.4. As we can see, J/ψ is located in a high-mass region and is made of charm quarks. This mass gives a scale that makes possible to use perturbative QCD at small x. Adding the fact of very narrow peak and the possibility of high energetic collisions, we can claim J/ψ to be very favoured particle for our analysis.

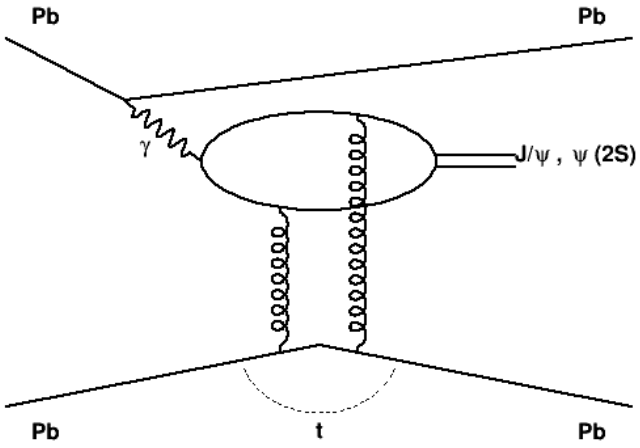

Figure 2.2: A Feynmann diagram of lead-lead ultra-peripheral collision, which produces J/ψ particle. The t stands for the transferred momentum. The γ is a quasi-real photon emitted from the Pb nucleus.

J/ψ **properties**	
Type	meson
Composition	charm quark and antiquark
Discovered	1974, SLAC and BNL
Mass	3.0969 GeV
Full width	92.9 keV
J^{PC}	1^{--}
Charmeness	0 (hidden charm)

Table 2.1: Properties of the J/ψ particle.

J/ψ **decay channels**	
Mode	Fraction (Γ_i/Γ)
hadrons	(87.7 $\pm$ 0.5) %
e^+e^-	(5.971 $\pm$ 0.032) %
$\mu^+\mu^-$	(5.961 $\pm$ 0.033) %

Table 2.2: The main decay channels of the J/ψ particle. Data taken from [9].

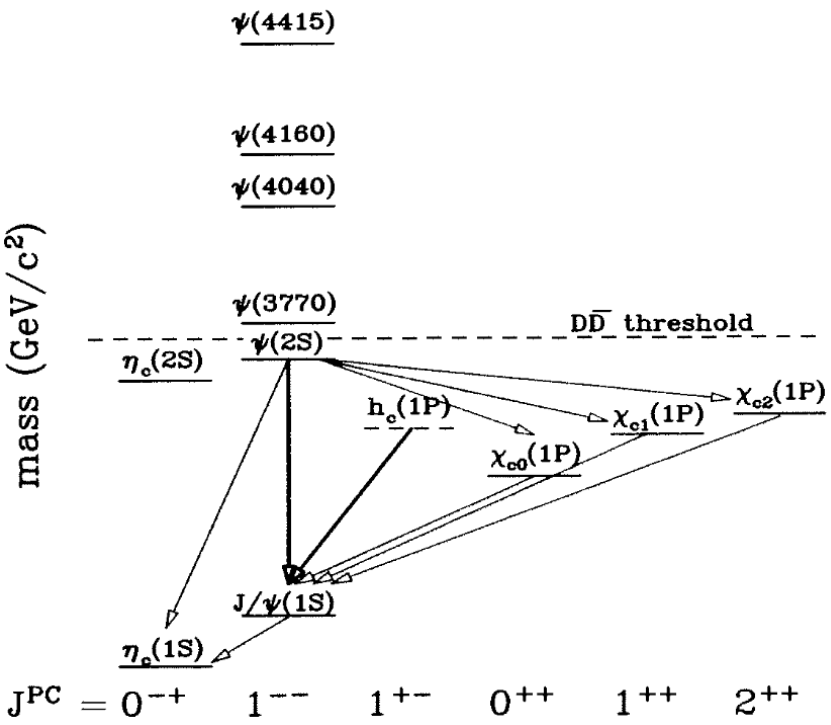

Figure 2.3: The charmonium family. Taken from [10].

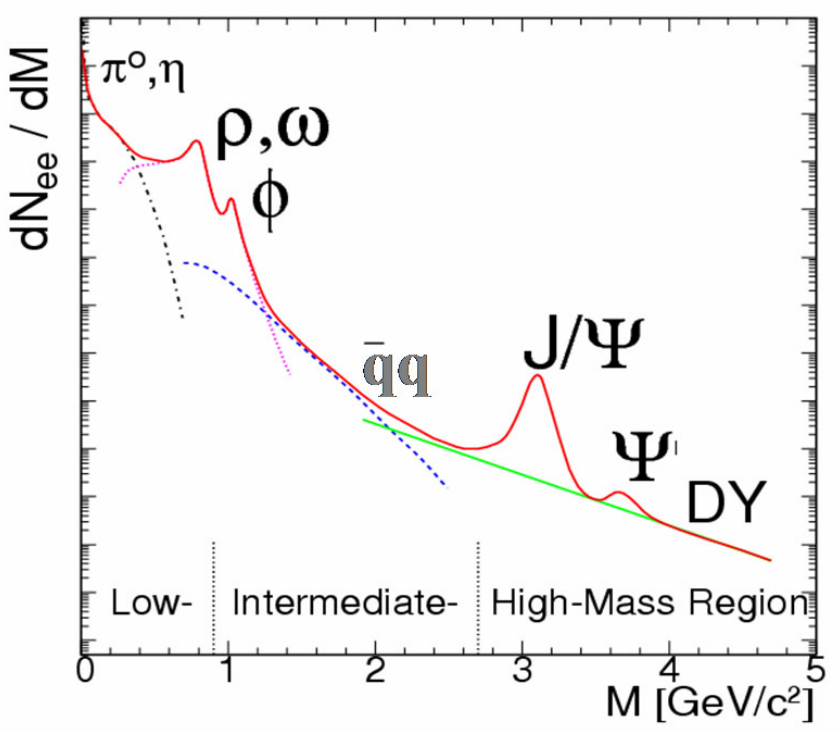

Figure 2.4: Dilepton mass distribution including the continuum and vector mesons. [11]

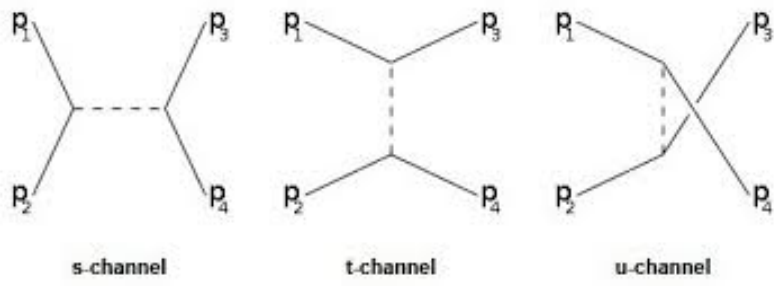

Figure 2.5: s- t- and -u Channels of scattering processes.

2.3 Mandelstam variables

For studies of kinematic of high energy physics new variables have to be defined. Some of them are so called Mandelstam variables. These are mostly used in scattering experiments, where we have 2 particles before an interaction and 2 particles after. All together we have 3 variables, which are labelled as channels (see Fig. 2.5) and are defined by Eq. 2.1. Their advantage is, that they are Lorentz invariant. Also in center-of-mass system they have clear meaning. The s-channel represents a square of the total energy of incoming particles. The t-channel reflects the momentum transfer between incoming and outcoming particle. The u-channel has a similar meaning. If we look again in the Fig. 2.2, one can clearly see, why we are interested in t-channel.

$$\begin{aligned} s &= (p_1 + p_2)^2 = (p_3 + p_4)^2, \\ t &= (p_1 - p_3)^2 = (p_2 - p_4)^2, \\ u &= (p_1 - p_4)^2 = (p_2 - p_3)^2, \end{aligned} \tag{2.1}$$

2.4 The cross section

A cross section is related to a probability of a particular event on an area. In particle physics is usually meant as a measure of the probability of interaction between two particles. In this thesis we study the dependence of the cross section on t for a reaction

$$Pb + Pb \rightarrow Pb + Pb(Pb^*) + J/\psi.$$

As we discused above, this process describes an interaction with a photon, therefore we speak about a photoproduction.

A total photoproduction cross section is

$$\sigma_x = \int d\omega \frac{n(\omega)}{\omega} \sigma_x^{\gamma}(\omega), \tag{2.2}$$

where we integrate a photon flux $n(\omega)$ and a photonuclear cross section over energies ω [6].

We are more interested in the photonuclear cross section. Using the model introduced by Adeluyi and Bertulani [7] we can write this cross section as

$$\sigma_{\gamma Pb}(y) = \left.\frac{d\sigma}{dt}\right|_{t=0} \Phi(y), \tag{2.3}$$

where

$$\left.\frac{d\sigma}{dt}\right|_{t=0} = C_V \frac{16\pi^3\alpha_s^2\Gamma_{ee}}{3\alpha M^5}[xG_A(x,Q^2)]^2 \tag{2.4}$$

and

$$\Phi(y) = \int_{t_{min}}^{\infty} dt|F(t)|^2. \tag{2.5}$$

Here Γ_{ee} is the decay width to electrons, $G_A(x,Q^2) = g_p(x,Q^2)R_g^A(x,Q^2)$, where g_p is the gluon PDF in the proton and R_g^A is the nuclear modification factor of the gluon distribution and $t_{min}(y) = (\frac{M^2}{4k\gamma_L})^2$ with γ_L the Lorentz boost of photon source. $F(t)$ is the nuclear form factor.

In our case we take the form factor as the Woods-Saxon distribution approximated as a convolution of a hard sphere and Yukawa potential with the range $r = 0.7$ fm [13]. Then the form factor looks like

$$F(q = \sqrt{|t|}) = \frac{4\pi\rho_0}{Aq^3}[\frac{\sin(qR_A) - qR_A\cos(qR_A)}{1+a^2q^2}], \tag{2.6}$$

where A is atomic number, ρ_0 is the nuclear density of the hard sphere, R_A is the radius of the nucleus and a is the range of the Yukawa potential.

Puting all things together the photonuclear cross section we are using have the form

$$\frac{d\sigma(\gamma + A \to V + A)}{dt} = NORM|F(t)|^2 \tag{2.7}$$

with $NORM$ standing for the normalization of the function.

More general way is to neglect the range of the interaction and as a form factor use exponential function

$$F(t) = e^{bt}, \tag{2.8}$$

where b corresponds to a transversal nuclear size as $b = \frac{1}{2}R^2$.

Chapter 3

Implementation

3.1 The analysis

To study the cross section of production of vector meson in UPC we have to choose a good data. An opportunity to measure such events at nowadays highest energy possible (at LHC facility) appeared in 2011. That year several runs with Pb-Pb collisions were set-up for ultra-peripheral collisions. The data we analyse were prepared in AOD train number 156. This root file contains a J/ψ tree with 1 135 296 events and ψ(2S) tree ready for further analyse.

Besides this data also Monte Carlo simulations (MC) were used. Three root files were made. One represents events, where J/ψ particle was produced coherently, another one is for incoherent production and the last one contains $\gamma\gamma \to \mu\mu$ events, which stands for the background. All of them have 2 trees identical with the measured data. Moreover both trees have two branches. One stands for generated particles and another one consists of data for reconstructed tracks.

3.1.1 Data selections

In order to find out the right events to fit, we had to apply additional selection criteria. We used three different types of selections. For measured data we used following cuts:

- all detectors worked properly
- event has been triggered with CCUP4
- nothing in V0
- ZDC energy < 500 GeV
- both particles are μ within 4σ identified by their energy loss (TPC)
- tracks have opposite charge
- criteria for Good Track are the following
  - track exists
  - filter bit 0 set

Cut	Events
no cut	1 135 296
trigger	1 135 296
V0	605 481
ZDC	203 051
TPC	172 399
opposite charge	119 602
Good Track	119 602
Mass	364
Pt	298

Table 3.1: Number of selected events for measured data.

  - track has been refitted with TPC and ITS
  - track in TPC has at least 50 clusters
  - at most χ^2 of 2 per degree of freedom
  - a point in SPD (a part of ITS)

- mass is between 3.0 GeV and 3.2 GeV
- $p_t < 0.13$ GeV

Reason for some selections are straightforward. We will mention only the condition for ZDC, which ensures that less than one neutron appeared in our selected processes and cut of transverse momentum, which exclude the region where diffraction peaks in the coherent production appear (see below). An impact of these criteria on the number of events can be found in the Tab. 3.1. At the end we have 298 candidates for further studies. This number of candidates correspond to those found in the independent analysis performed for [1].

For MC simulations we have two different selection criteria. One for generated particles and the second one for reconstructed tracks. For generated sample we used this criteria:

- at least 2 generated particles
- rapidity of $\mu^+\mu^- < \pm 0.9$
- $p_t < 0.13$ GeV
- both generated particles are μ

The effects of the cuts is in the Tab. 3.2.
The last selection criteria were used for reconstructed tracks and are listed here:

- exactly 2 tracks have been reconstructed
- application of the same selection criteria as for generated particles

Cut	Events
no cut	1 382 193
2 generated particles	1 381 792
rapidity	1 249 818
Pt	1 215 114
both muons	1 215 086

Table 3.2: Number of selected events for MC Coherent sample - generated particles.

Cut	Events
no cut	341 700
2 reconstructed tracks	170 850
criteria for generated particles	163 074
trigger	163 074
V0	163 036
ZDC	162 877
TPC	161 030
opposite charge	161 030
Good Track	161 030
Mass	160 793

Table 3.3: Number of selected events for MC Coherent sample - reconstructed tracks.

- application of the same selection criteria as for measured data

As one can see, they are composed of criteria introduced before. The reason, why we include criteria for generated particles, is to avoid wrongly simulated events, where i.e. 2 reconstructed tracks were made, but 2 generated particles weren't. Because we want to use MC simulation to find the best fitting model, we had to inherit the same selection criteria as for measured data as well. Impact of this selection process on the number of events is in the Tab. 3.3.

We have to denote, that numbers of events of MC Coherent sample differ from the incoherent and background ones. In fact, these numbers have only informational character and we will not introduce all of them here.

3.2 A work-flow

In this paragraph we will briefly describe each part of the analyse we did. The conclusion and results of this will be presented later.

3.2.1 Basic plots

In the beginning of our analyse we had to decide, which selection criteria we will use. For this reason it is crucial to study some basic distributions. Our main goal is to study J/ψ particle, so we have to constrict a mass sector of our data. For this we looked at the mass distributions. These can be found in Figs. 3.1 and 3.2. In the Fig. 3.1 one can see dimuon distribution for measured data. There is a strong peak around 3.1 GeV which is considered to be a sign of J/ψ particle. But there is also a background which we have to constrain. In the other panels are informations about generated particles, in other words the input parameters for our simulations. In Fig. 3.2 we show already processed data. For measured data it means that cut for mass was applied. The MC data show reconstructed tracks. With reconstructed tracks we mean a data, which would ALICE detector collect, if our generated particles would be produced in ALICE's interaction point. Therefore a "J/ψ peak" for coherent and incoherent sample change its shape from sort of delta function to Gaussian one.

A next quantity we focused on is a transversal momentum, displayed in Figs. 3.3 and 3.4. First interesting thing in Fig. 3.3 is the top right panel, where sample of coherent production of J/ψ particles is shown. This process embodies a strong diffraction pattern, which is an unwanted effect for the studies we wanted to perform, because it produces structures in the efficiency distributions. Methods, how to deal with this problem, exist, but due to low statistic we are more interested in low p_t and therefore we added the p_t cut in our selection criteria. One more thing we can obtain from the Fig. 3.3 is the fact, that our measured data actually are a sum of all three MC samples. In Fig. 3.4 we introduce the measured data with p_t cut. But transversal momenta of all mentioned processes populate this p_t region. Therefore we have to be careful, extract the background in further analysis and remember effects of the rest processes during an interpretation of our results.

At last we have the main goal of our study - transferred momentum t. Neglecting the momentum of photon from Fig. 2.2 we can replace this with the transverse momentum of the J/ψ particle squared. Appropriate plots are in Fig. 3.5 and 3.6. Those are the data we want to use. The left top panel of the Fig. 3.6 are our measured data before the subtraction of background. Now we have around 298 events which should decrease a little bit. This predicts, that the fit will be with a big error. Therefore we applied some other analytic methods to improve our results.

3.2.2 The acceptance vs. efficiency procedure

As it was pointed before the reason why we have Monte Carlo simulations is to have samples with larger statistics, where we can test our methods. Our MC data are divided to two groups - generated particles and reconstructed tracks. Because we want to correct our measured data for efficiency of our detector, we have to somewhat compare these two groups.

The acceptance vs. efficiency is a simple procedure, where we divide p_t^2 distribution of reconstructed tracks by p_t^2 distribution of generated particles. Using this result on our measured data we should get back an actual distribution in our collisions.

In our analyse we follow quite straightforward steps. Both distributions had to undergo the selection criteria mentioned above. Then a new histogram is made. And finally, a fraction of both distributions is stored in it for future purposes.

3.2.3 The efficiency and purity procedure

In order to account that we have only a few hundred events, we plan to extract the t distribution using only four t-ranges. It means we have to sort our events into 4 bins. Because our distribution has exponential character, we expect a strong migration from low p_t region to higher ones. Therefore we used this procedure to check, if regular binning is good enough or we have to prepare the distribution with variable binning.

What we want to study is by how much the transferred momenta of generated particle (Gen Par) and reconstructed track (Rec Trk) differ in one event. Therefore we prepared a sample, where we have the same number of Rec Trk and Gen Par - on both were applied selection criteria for Gen Par and Rec Trk. The next step is to put everything in the graph.

First we aimed on the efficiency. Now, we are dealing with 2D histograms. In this both axises are divided according to the binning. The x-axis represents p_t of Gen Par, meanwhile y-axis stands for a combination of Gen Par and Rec Trk. For example in box [2,1] is stored a fraction of events, where Gen Par p_t was in the bin 2, but Rec Trk p_t was in the bin 1, and events, where Gen Par p_t was in the bin 2. In other words we have a fraction of events, where p_t migrates from bin 2 to bin 1 during the analysing process.

The purity is the same procedure, but on the x-axis we have p_t of Rec Trk instead. As the name of it suggests, these numbers show, how pure our reconstruction is.

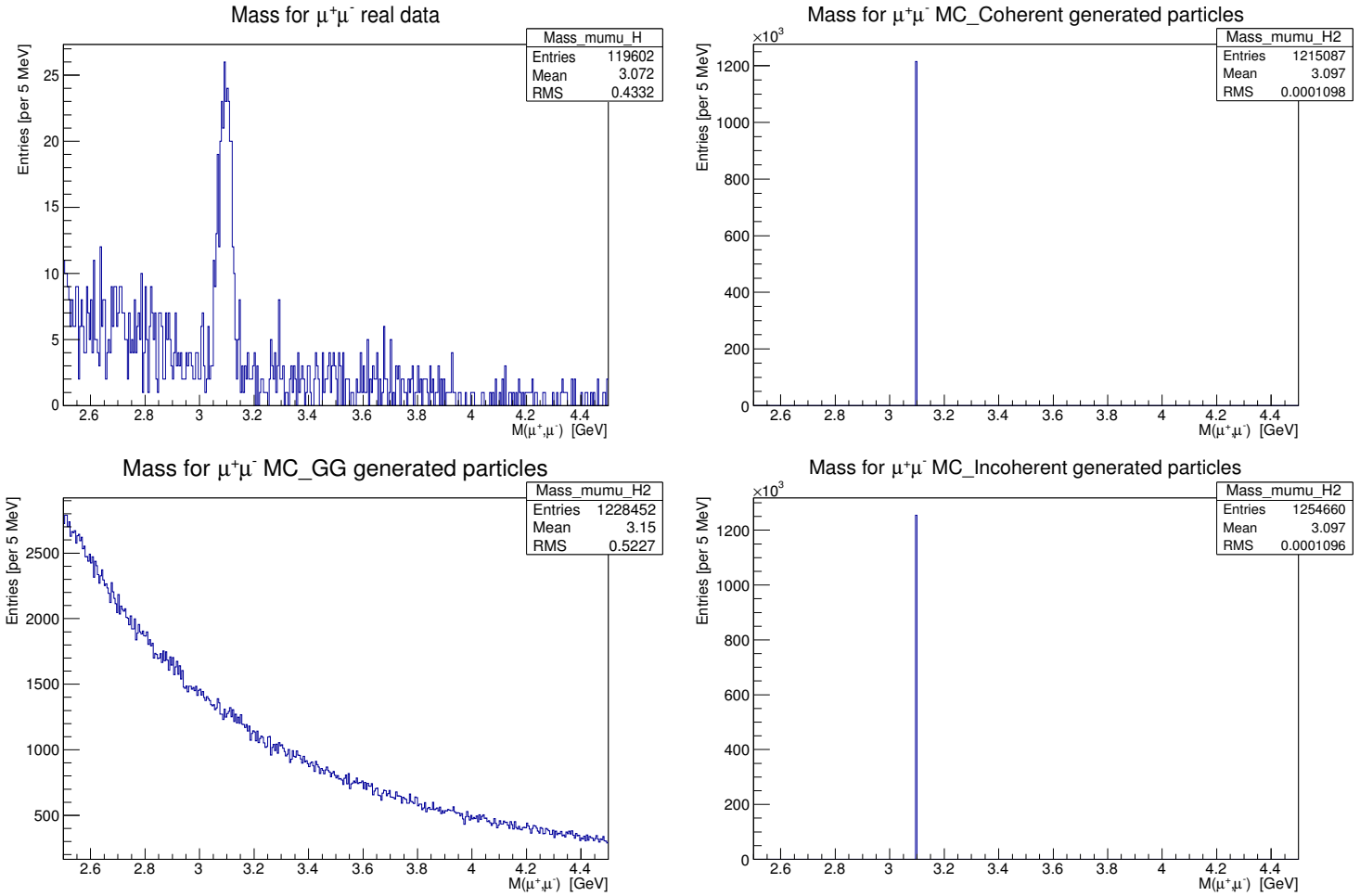

Figure 3.1: (From the left to the right) Plots of mass distributions for measured data, MC coherent sample, MC background and MC incoherent sample. MC show generated particles.

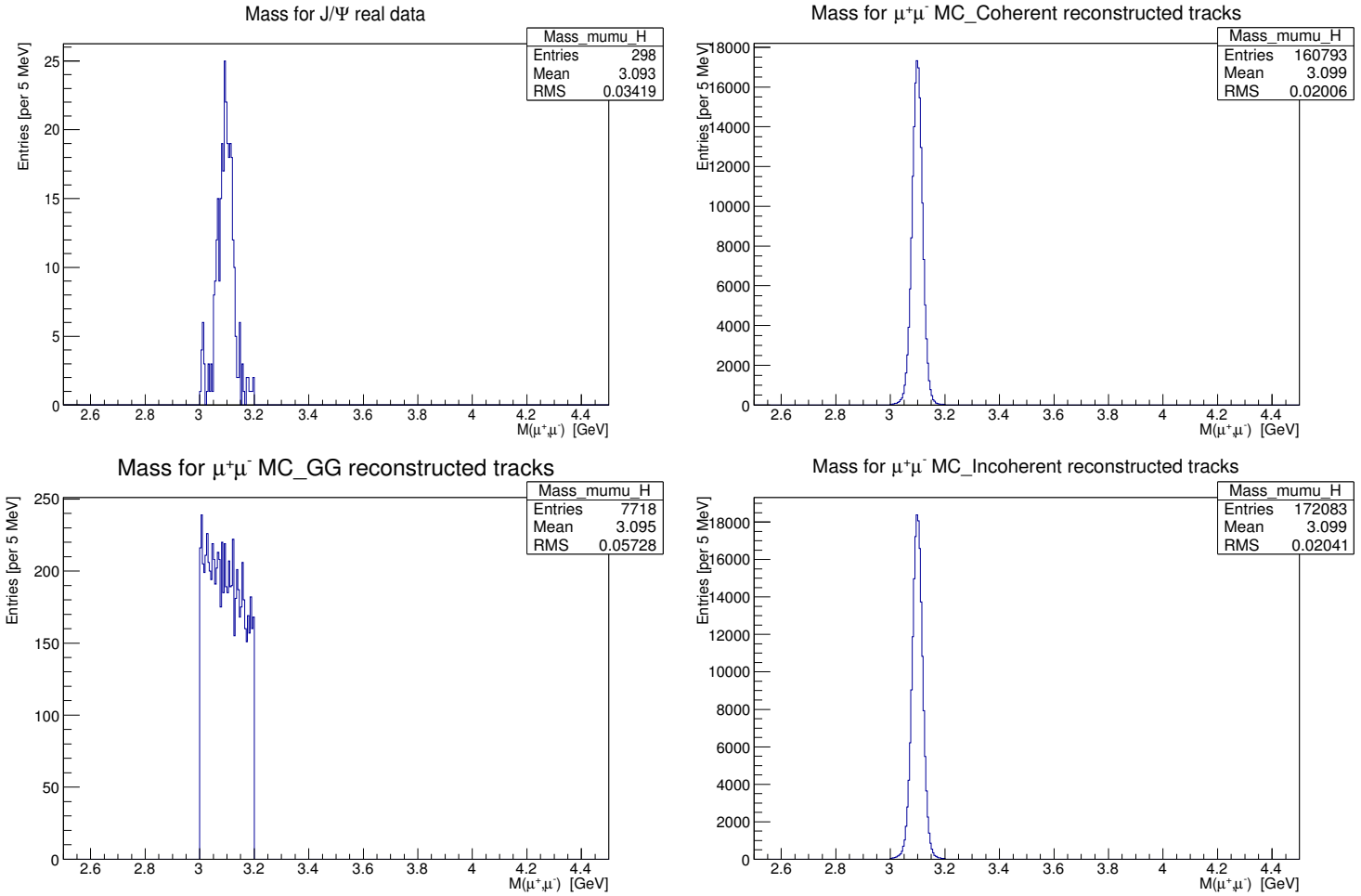

Figure 3.2: (From the left to the right) Plots of mass distributions for measured data, MC coherent sample, MC background and MC incoherent sample. The mass selection criterium was used. MC show reconstructed particles.

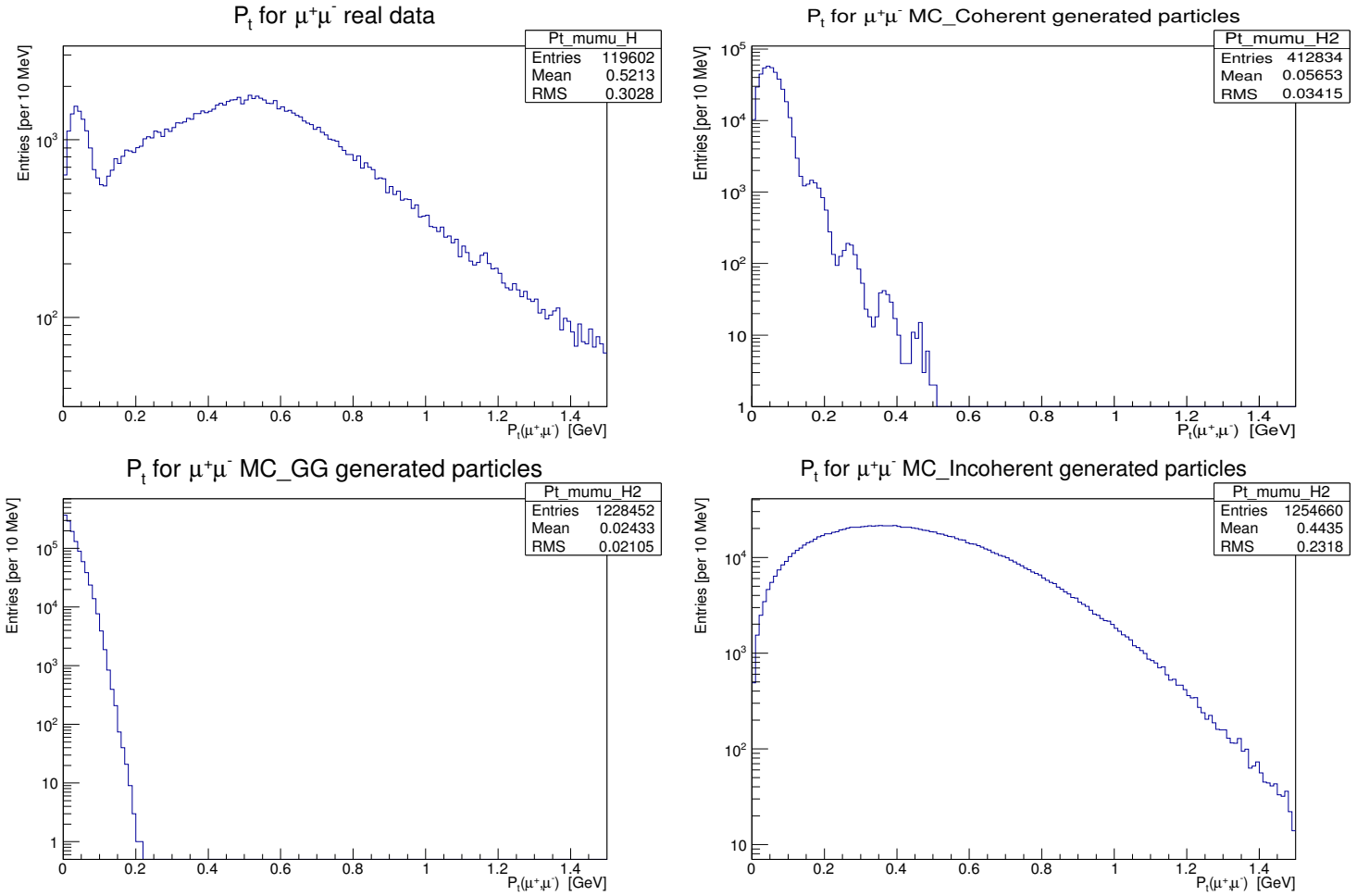

Figure 3.3: (From the left to the right) Plots of p_t distributions for measured data, MC coherent sample, MC background and MC incoherent sample. MC show generated particles. No p_t cut used.

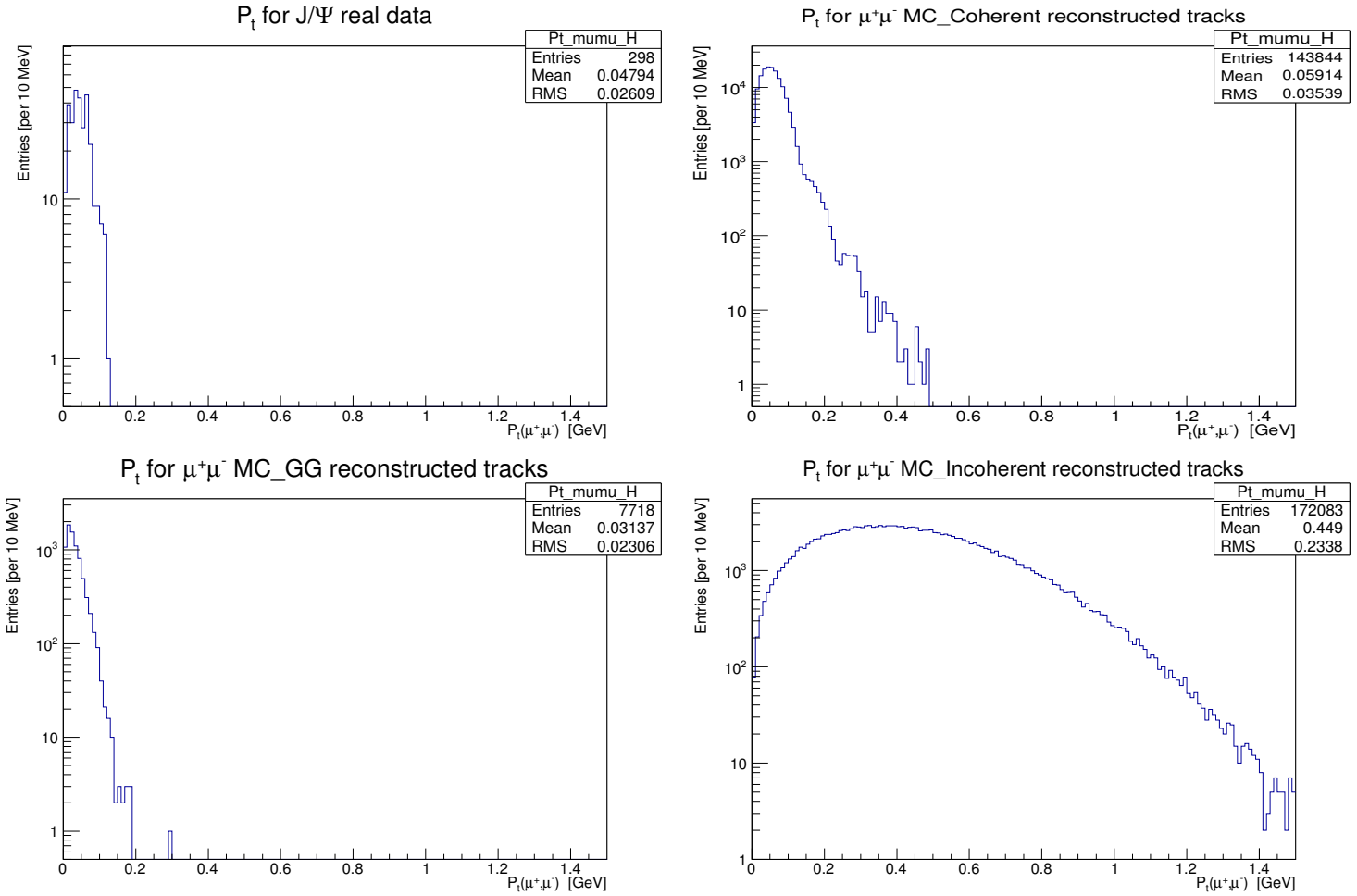

Figure 3.4: (From the left to the right) Plots of p_t distributions for measured data, MC coherent sample, MC background and MC incoherent sample. The mass selection criterium was used. MC show reconstructed particles without p_t cut.

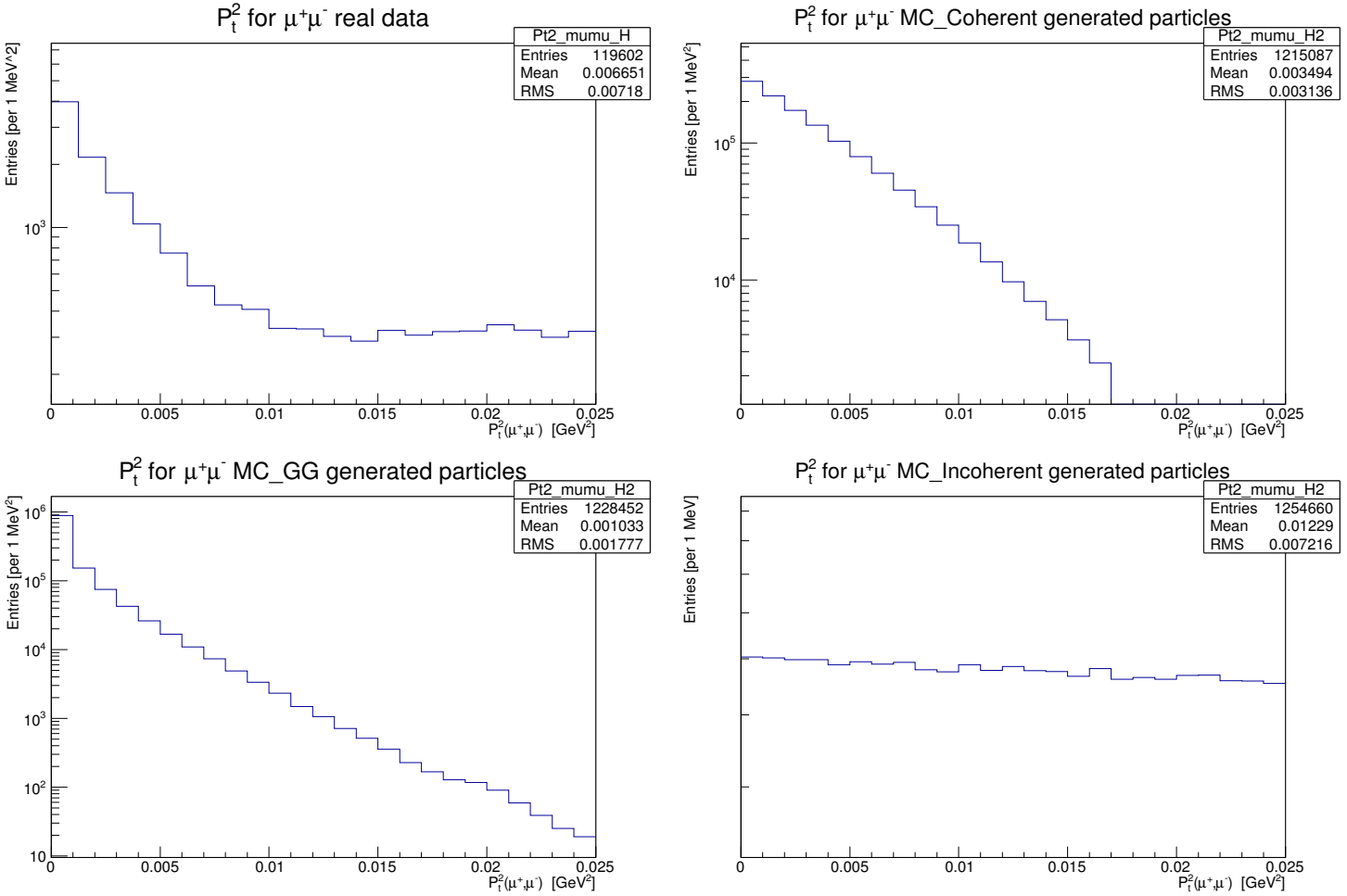

Figure 3.5: (From the left to the right) Plots of p_t^2 distributions for measured data, MC coherent sample, MC background and MC incoherent sample. MC show generated particles.

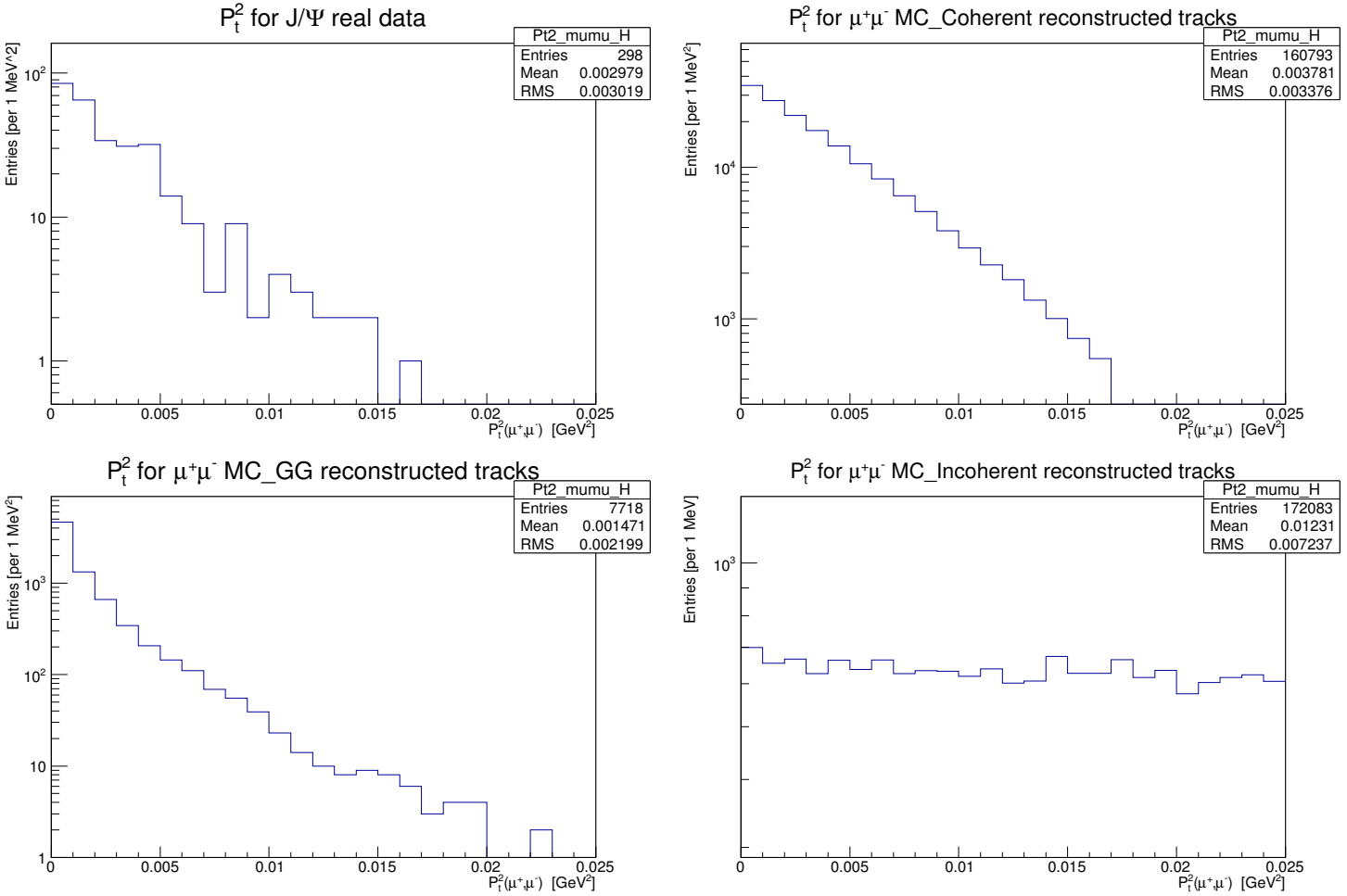

Figure 3.6: (From the left to the right) Plots of p_t^2 distributions for measured data, MC coherent sample, MC background and MC incoherent sample. The mass selection criterium was used. MC show reconstructed particles.

3.2.4 Fitting procedure

The following study is performed using MC events from the coherent sample. In principle, one should select candidates in a given bin, fit the mass distribution and subtract the contribution from background and finally apply the correction for acceptance and efficiency. As we are using a MC without background it is easier to just count the number of events per bin and use this to fit the t distribution.

The fit cannot be obtained directly from the histogram, because ROOT proceed as follow: It takes a middle of the bin as a point for the fit and calculate horizontal errors as a width of the bin. This is not correct, because of the exponential behaviour of the expected fit. There is more events in the left half (lower p_t) of the bin than in the right one. Therefore we have to store all data using TGraph function. This procedure slightly differs for generated particles and reconstructed tracks.

The first part is the same for both. We applied appropriate selection criteria and classified the data according to their p_t^2 to several boxes. In each box we stored number of events and the sum of all transferred momenta divided by the number of events. The first is for computation of a vertical error, the second serves as our fitting point.

To prepare a graph of reconstructed tracks similar to the measured data corrected for the efficiency of the detector, we had to add new informations we got from acceptance vs. efficiency procedure and efficiency and purity procedure. This is simple as it sounds. After the first step described in the previous paragraph we took the efficiency of the reconstruction for each bin and divided it. The next task is to define 4 bins and resort our p_t^2 boxes. Values in the bins have to be divided by their width to get correct numbers.

Once these graphs are stored, we only have to fit them to get results. As a fit function we used 2.7 with a form factor 2.6. We had 3 free parameters - a, R_A and $NORM$ - with options to fix R_A and/or a.

At the beginning we wanted to fit only the coherent sample, divide it to several smaller samples and check, if we are able to get nice results this way. Then we repeat the whole process, but we add other two samples to our source data. After the analysis of this complete MC data we should have something, which could be considered as an "artificial" measured data. Once we are satisfied with this fits, we apply it on the "real" measured data. Unfortunately, as will be shown in the next chapter, the procedure was already problematic with the pure coherent sample, so we only studied, up to now, this case.

Chapter 4

Discussion and results

4.1 The correction for the acceptance and the efficiency

As it was described above, we had to use our Monte Carlo data to correct measured data. Results can be found in Fig. 4.1. The best shape of the ratio would be a flat distribution. If we take into account the errors, the ratio of incoherent samples fulfils this expectation. The other samples are a different story. As we can see, the detector is more efficient for higher p_t. For the coherent sample the explanation could be, that one of the muons from low-p_t J/ψ didn't hit the detector, because these muons should be more back-to-back (their momenta should be more equal with opposite sign). But this isn't a problem for our analysis. Strange behaviour expresses the background. As we can see, we have more reconstructed tracks in the high-p_t region than generated particles. The behaviour of the sample at large p_t is explained by the very few events there and migrations from lower p_t where there are many events, producing an efficiency larger than one, i.e. we are measuring events where no event was produced.

4.2 The best binning

Another feature we were interested in was the size of the bins we would use for a construction of the fit points. The efficiency and purity procedure was used for this. In Fig. 4.2 we can see a result of this analysis with regular binning, where every bin has a width of 0.005 GeV^2. An outcome of this is very poor. We have a yield of less than 70% in the second bin and it goes under 50% in the last bin. Therefore we tried many other configurations of the variable binning and we came up with the one, which is shown in Fig. 4.3. All of the bins conserve at least 70% and the last bin almost 80%, which is an important result under the strong limitation of low statistic in high p_t. Therefore we chose the binning to be: 0.001 GeV^2, 0.003 GeV^2, 0.004 GeV^2 and 0.008 GeV^2. We have also performed these calculations for 5 bins, which brought some promising results, but we have decided to stay with 4 bins issue and kept this possibility for future analyses.

4.3 The fit of the Monte Carlo coherent J/ψ sample

To compare several fits we have decided to split this sample to several smaller ones. Because we want to also examine a possibility of fitting our measured data, we prepared samples with a similar number of entries. Tab. 3.1 tells us to fit samples with 300 entries which bring us to the final number of 539 samples. A real number of entries in each bin is increased due to an application of the correction for the acceptance and the efficiency. Examples of this fits with different numbers of fixed parameters are shown in Figs. 4.4, 4.5, 4.6. To satisfied the used model (Eqs. 2.6 and 2.7) we wanted to achieve the values $a = 0.7$ fm and $R_A = 6.62$ fm [13]. We should also state that all used fits converged.

If we didn't fix any parameter, we got an average value over all samples of a for generated particles 1.16 ± 0.04 fm. For reconstructed particles we got similar result of 1.29 ± 0.11 fm. Even if we envisage an error of this numbers, we are still far from the expected value. To complete the story of unsuccessful fit, we have to also mention the wrong values of R_A, which are 5.87 ± 0.04 fm and 5.39 ± 0.11 fm for generated particles and reconstructed tracks respectively.

Therefore we have decided to fix the parameter a to a value 0.7 fm and we paid our attention on R_A. For both generated particles and reconstructed tracks we got a better average numbers (6.22 ± 0.08 fm for generated particles and 6.09 ± 0.23 fm for reconstructed tracks) closer to the expected one. But it was still outside our error. Also if we look at the Fig. 4.5 we see the fit goes wrong for higher p_t^2.

The last results are the fits with both parameters fixed. Now we could only compare normalizations of the generated particles and reconstructed tracks, which should get the same numbers. Somewhat these two numbers do agree. Unfortunately, if we look at the Fig. 4.6 and check the plots of the fit, we see, that this line doesn't correspond with our data at all.

All these informations brought us to an important conclusion, that the model we used for our data is not correct. The reason can be, that this model is for t as a sum of the J/ψ p_t^2 and the virtual photon p_t^2. In our interpretation we neglect the second part, because we hope, that this is very small. Now we know we should be more careful in this matter.

Therefore we have decided to apply more general way. As a fit function we used Eq. 2.8. Examples of this fits are shown in Fig. 4.7. Resulting values of the b parameter are -256 ± 21 GeV^{-2} and -297 ± 8 GeV^{-2} for reconstructed tracks and generated particles respectively. Using natural units we have a transversal nuclear radius 4.5 ± 1.3 fm and 4.8 ± 0.8 fm respectively. These values are lower than we expected.

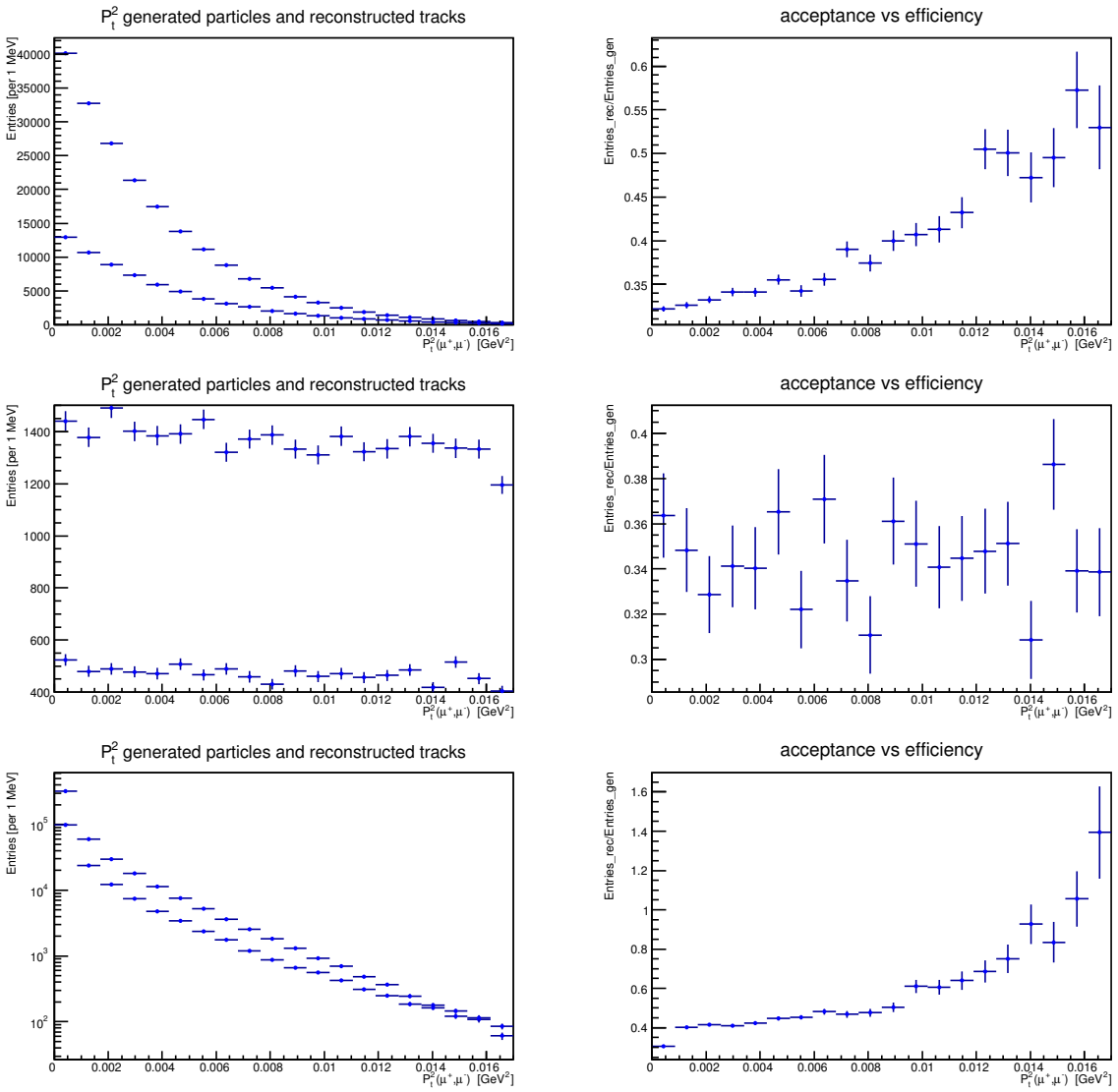

Figure 4.1: Plots of the p_t^2 distributions for generated particles and reconstructed tracks (left panels) and their ratios (right panels) for (from top to bottom) coherent J/ψ, incoherent J/ψ and background samples. On the left panels the top distribution are always for the generated particles.

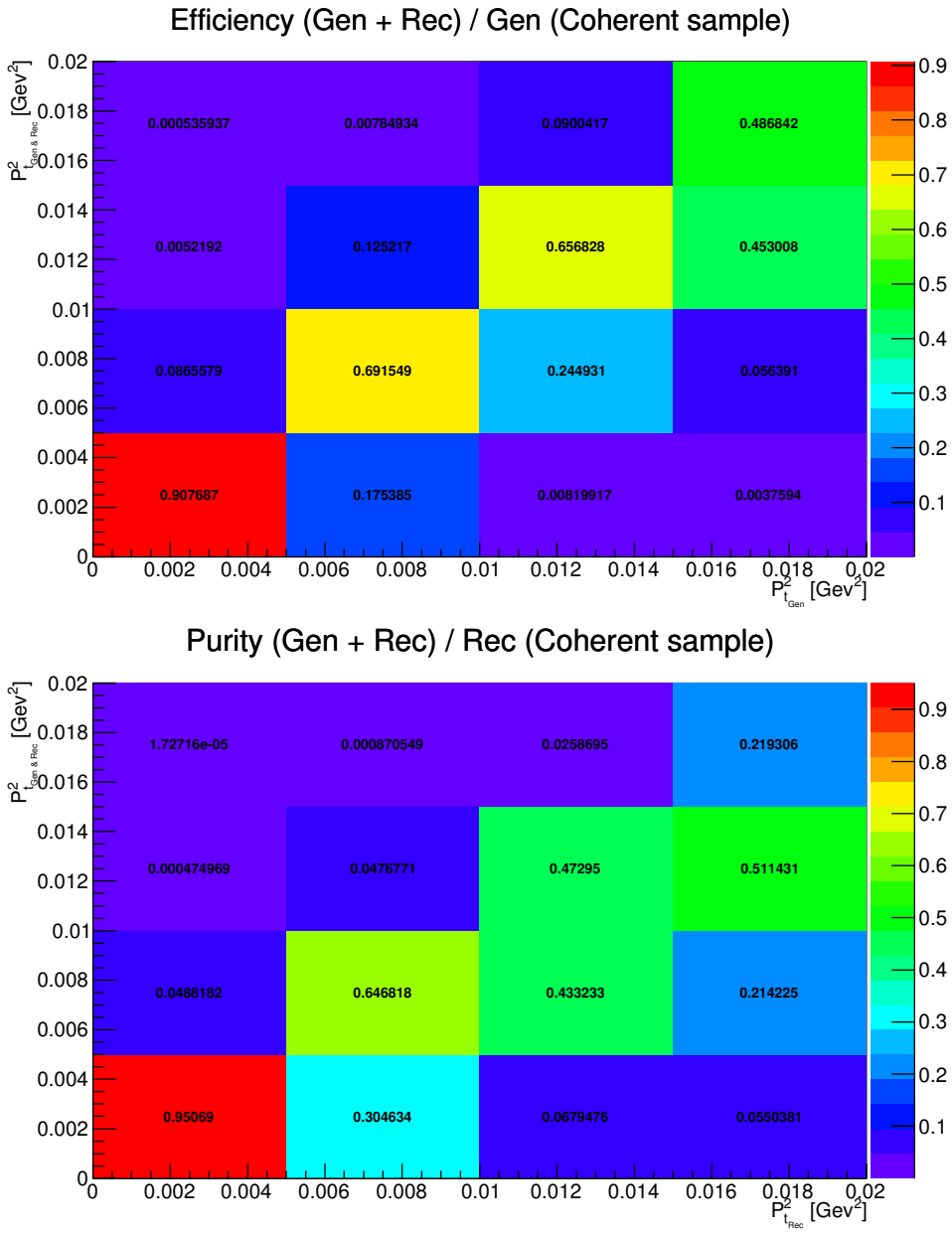

Figure 4.2: The efficiency and the purity with regular binning for coherent J/ψ sample.

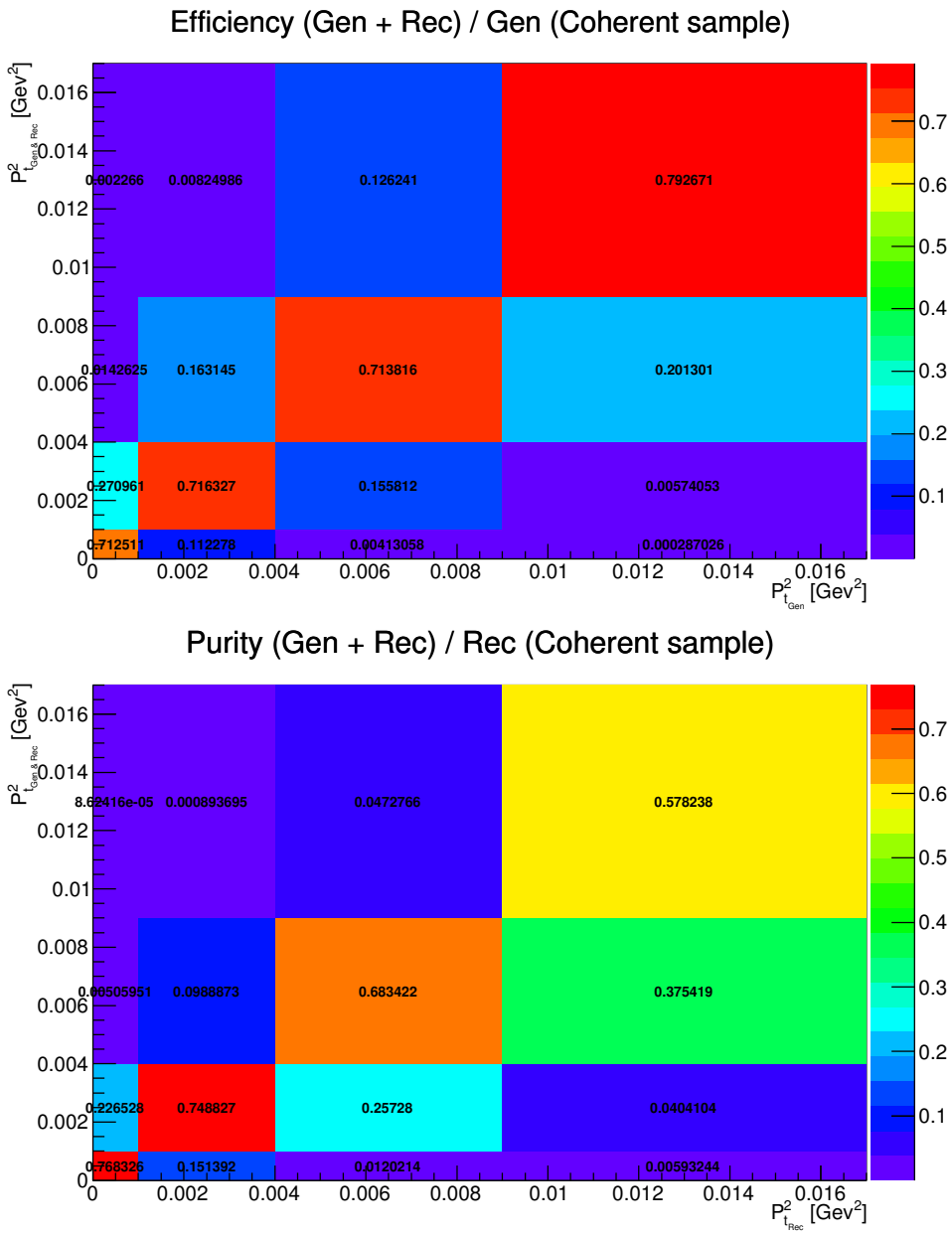

Figure 4.3: The efficiency and the purity with variable binning for coherent J/ψ sample.

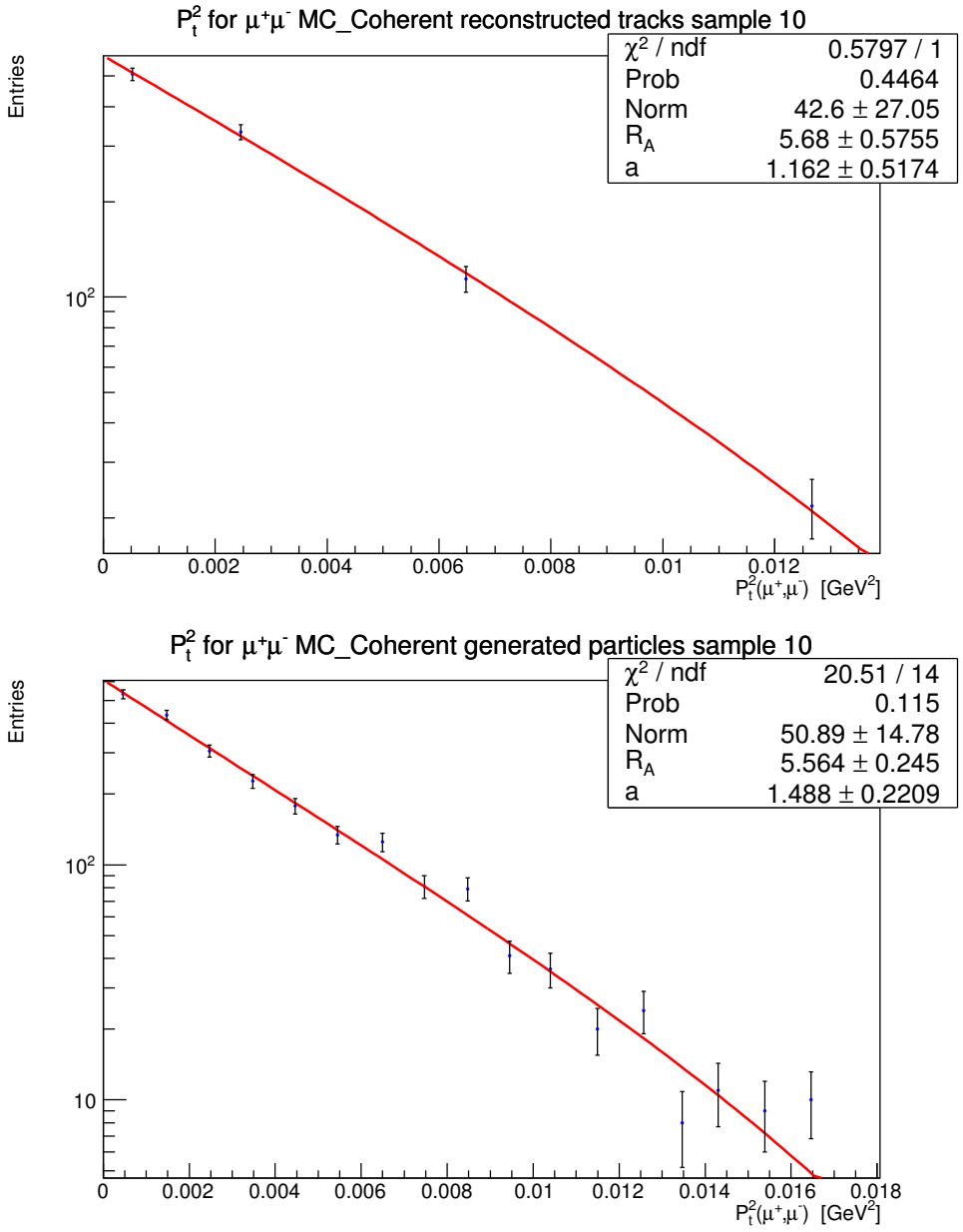

Figure 4.4: A fit of the p_t^2 distribution of the coherent J/ψ sample for generated particles and reconstructed tracks using Eq. 2.7 with all parameters free.

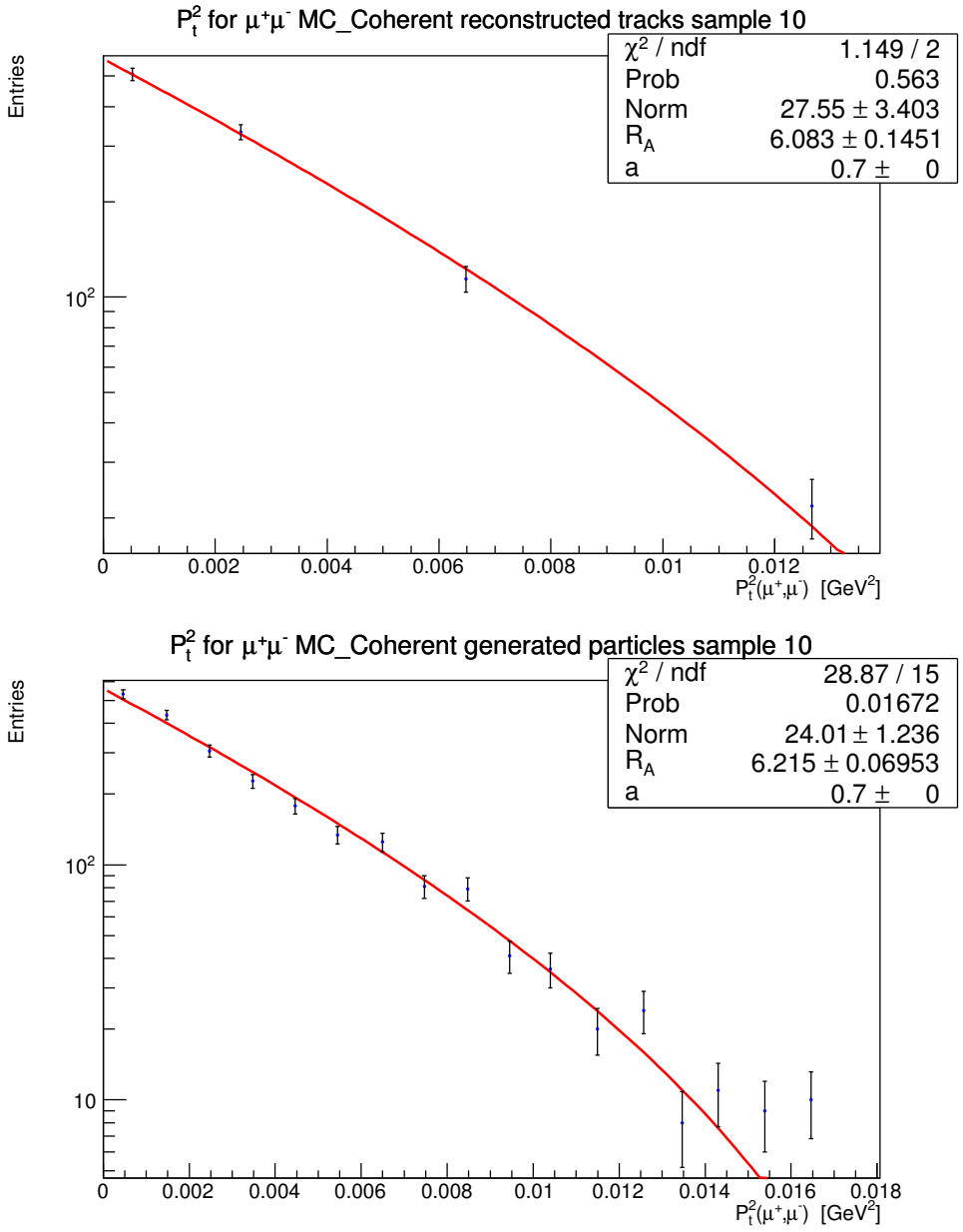

Figure 4.5: A fit of the p_t^2 distribution of the coherent J/ψ sample for generated particles and reconstructed tracks using Eq. 2.7 with a fixed parameter a.

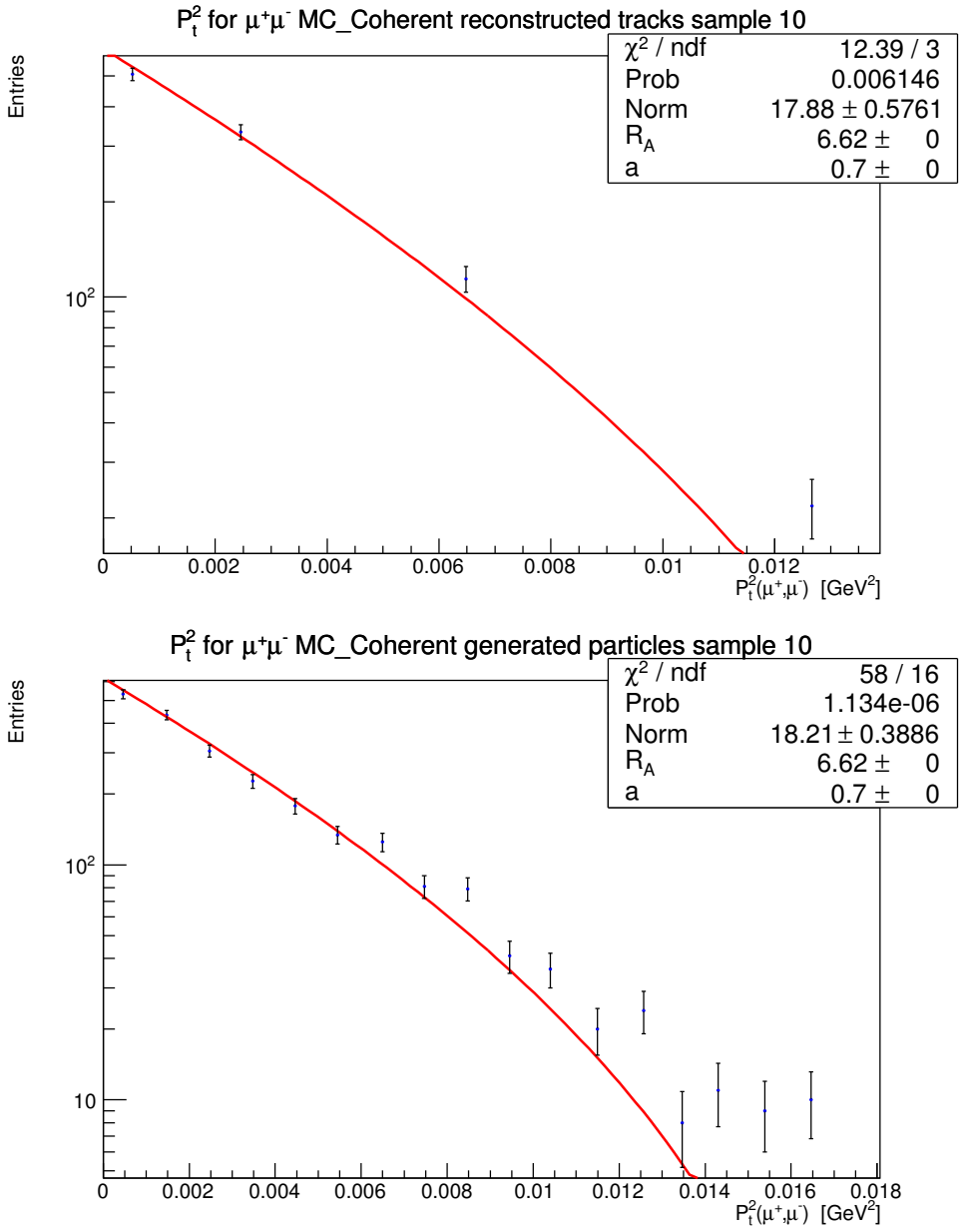

Figure 4.6: A fit of the p_t^2 distribution of the coherent J/ψ sample for generated particles and reconstructed tracks using Eq. 2.7 with fixed parameters a and R_A.

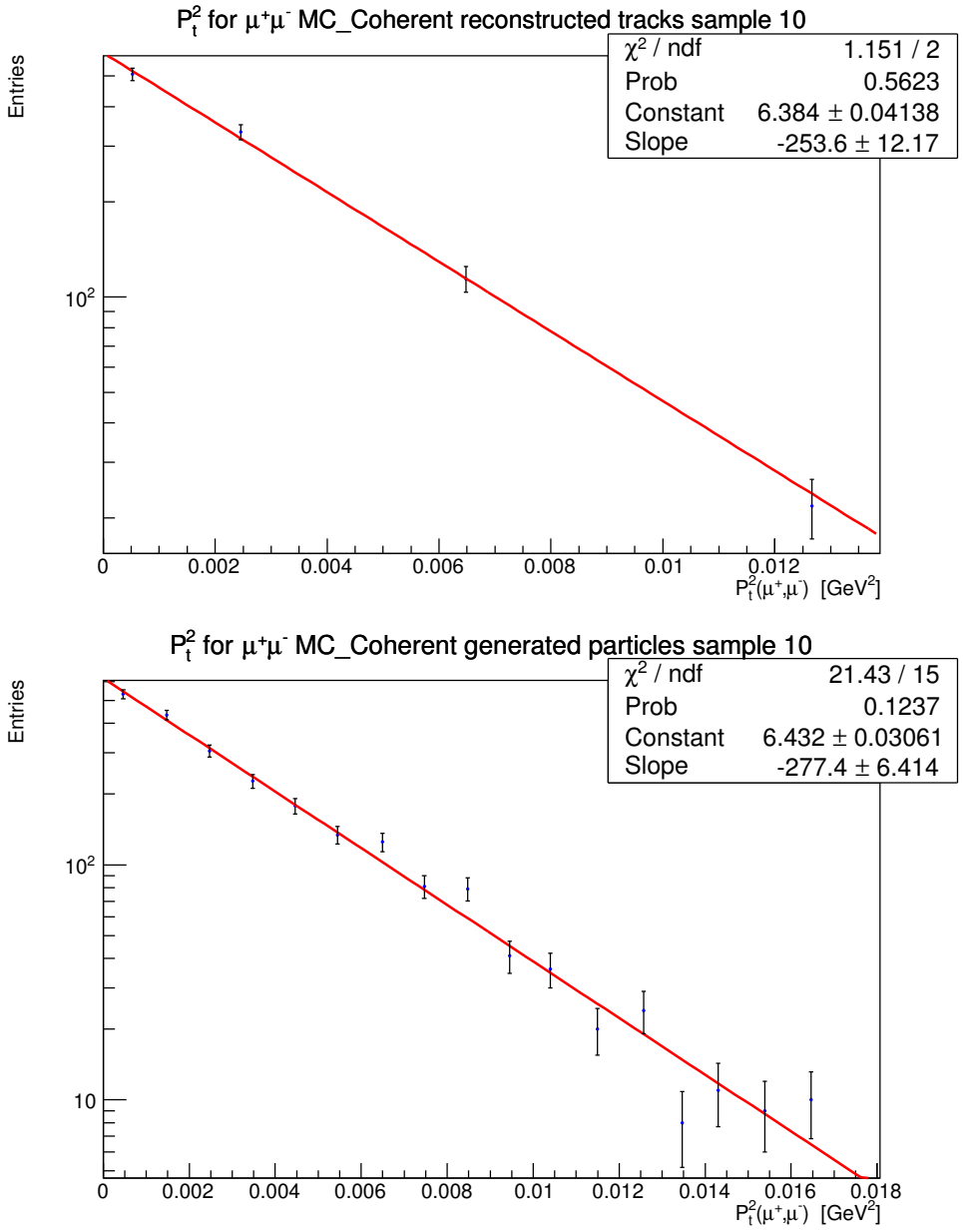

Figure 4.7: A fit of the p_t^2 distribution of the coherent J/ψ sample for generated particles and reconstructed tracks using Eq. 2.8.

Chapter 5

Luminosity computation framework

During the summer 2015 we developed the luminosity computation framework for the ALICE collaboration under the supervision of the ALICE trigger coordinator Evgeny Kryshen. Next lines document this work.

5.1 Introduction

Since the LHC has become operational in 2010, the experiment ALICE gathered a lot of physics data, which needed to be analysed. One of the intrinsic inputs for the physics analyse is a luminosity for different trigger classes. Unfortunately, in LHC Run 1 this was not provided by collaboration centrally and everyone had to spend extra time on this topic. For the LHC Run 2 we have prepared a new luminosity calculation framework.

A motivation of this effort is to provide a unified and precise luminosity source for ALICE analyses, which can be easily accessed in various formats. This needs a sort of automatic program, which will be periodically launched. A unix-based software utility Cron is used to manage it. Also run/trigger coordinators need up-to-date information. The goal is to provide them actual summaries on collected statistics for different LHC periods.

5.2 Theory

To understand the whole concept of this work, we have to describe the ALICE trigger system. A main part of the system is a Central Trigger Processor (CTP), which receives signal (input) from triggering detectors, makes a decision and sends a signal to readout detectors. There are 4 levels of decisions (LM, L0, L1, L2). An application of each of them depends on a speed of propagation of the signal from the triggering detectors to the CTP. Each level has two sets of counters. First, the CTP counts the number of events, LXB, satisfying logical combinations of trigger inputs in a predefined subset of bunch crossings (BC mask). Then an electronic veto, mainly due to busy detectors or downscaling, is applied and results are stored as LXA. Note, that B and A stand for (B)efore and (A)fter veto and X for the level of decision [12].

A well-arranged organization of these signals is crucial for handling these data. Objects, which group readout detectors, are called **clusters**. These have various names and due to hardware conditions we can have only 6 of them per a run. Another objects called **classes** group

several trigger informations like descriptor (logical combination of trigger inputs), BC-mask or cluster name. Each class contains informations about LXX counters, which is used for luminosity calculation. In order to improve this calculation new objects called **aliases** are introduced in the developed framework. Their job is to point to a class with the most precise triggers counts in the trigger cluster [14].

$$L_{Class} = \frac{R^B_{REF}}{\sigma_{REF}} F(\mu_{REF}) \frac{R^A_{Class}}{R^B_{Class}} D \tag{5.1}$$

Eq. 5.1 shows the formula, which is used for luminosity calculation. To calculate luminosity one has to know a cross section. Unfortunately this one is not known for every subdetector of the ALICE detector, therefore we have to use a reference detector T0, from which we extract reference trigger counts R^B_{REF}, which are connected with L0B or LMB decisions, and the reference cross section $\sigma_{REF} = 39$ [mb], which was estimated for proton-proton collisions at 13 TeV. In August 2015 the Van der Meer scan for the energy of 13 TeV was done and results will be added to the code.

The reference trigger counts have to be also corrected for the pile-up, which is done by the pile-up function $F(\mu_{REF}) = N\frac{\mu_{REF}}{R_{REF}}$, where N stands for the number of bunch crossings and μ_{REF} is an average number of collisions per bunch crossing. In addition, correction for a fake coincidence in T0A and T0C.

Because we want to calculate the luminosity for each class, we have to compute so-called lifetime of the class first. This is done by the ratio $\frac{R^A_{Class}}{R^B_{Class}}$, where trigger counts of the L2 decision level are taken. We have introduced the aliases in our framework, which means that for each class we replace used trigger counts with a different, more precise ones. But the classes from the same cluster can have a different downscaling factor. Therefore a variable D is also defined in Eq. 5.1 and stands for the ratio of downscalings of the original class and the alias class.

5.3 Implementation

A program which can extract informations from OCDB files, calculate luminosity and produce graphical output in various format was built. This consists of several macros written mostly in C++ language. Their dependency tree is shown in Fig. 5.1. A control macro, which inherits all files is named *runCollectTriggerInfo.C*. It can be run in 4 different modes, depending on which value of an argument (switch) is used. A default argument '0' is used to run standard mode, where a list of runs, which will be analysed, is extracted automatically to the file *addtolist.txt*. An argument '1' uses as an input a list of preselected runs, which are written in a file *selectedrunlist.txt*. Other two switches can be used for testing, where the program with an input argument '2' uses a short list of chosen runs (from different periods) and an argument '3' serves only for a single run level diagostic.

The most important is the default setting of the program. This will first run an *updateRunList.C* macro. Its job is to mount a source of OCDB files via cvmfs, extract names of all runs in the source folder, using a list of already analysed runs from *runlist.txt* choose non-analysed (new) ones and returns a list of them in the file *addtolist.txt*.

Next a loop over new runs is initialized. For each new run a macro *collectTriggerInfo.C* is started. This is the part of the code, where luminosity calculation is done. The OCDB files

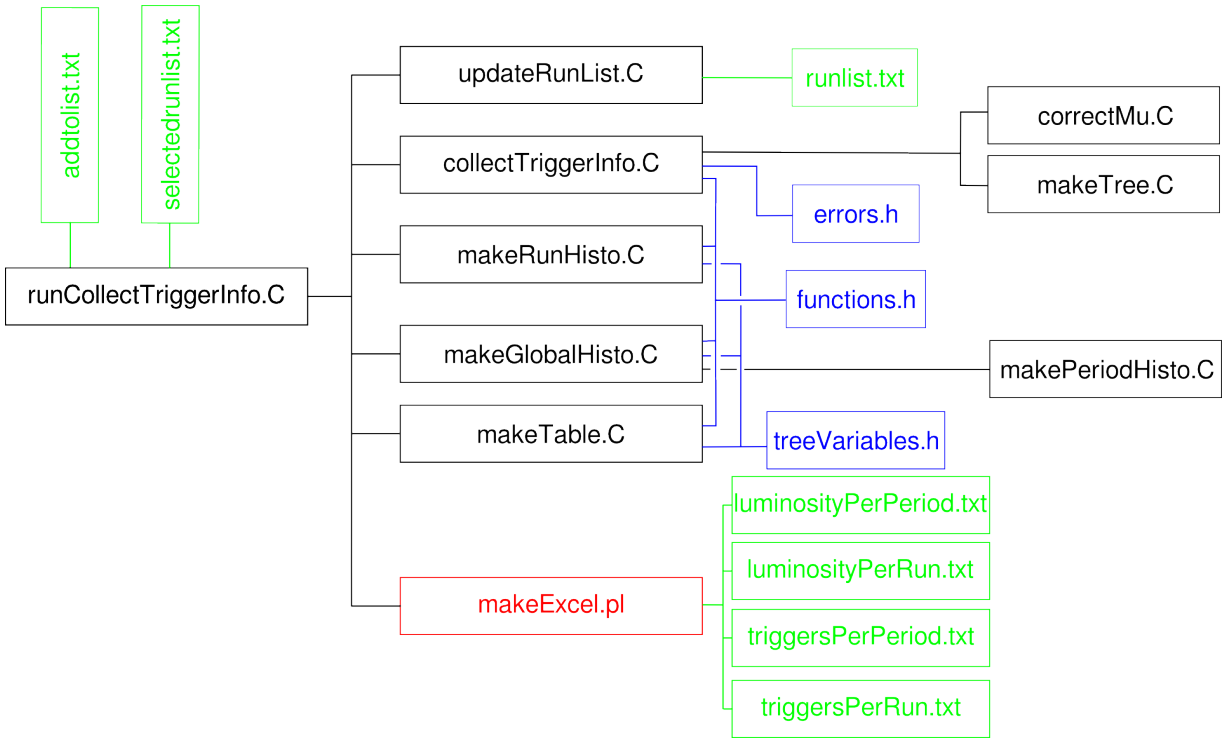

Figure 5.1: A dependency tree of the code. Objects functionalities are explained in the text.

are used as a source of informations needed for the calculation as mentioned above. In order to make the code better readable headers *errors.h* and *functions.h* are provided, which contain error messages and various subprocess functions respectively. A macro *correctMu.C*, provided by Martino Gagliardi, is used for a computation of the μ. In the end this macro calls *makeTree.C*, which saves all extracted and computed informations to a *ROOT* file in a TTree structure on a run level[15].

Another macro called *makeRunHisto.C* is triggered in the loop. A purpose of this one is to make a run level output, which means, that it creates a folder, where all files connected with the specific run will be stored and run level plots are made. Here, headers *functions.h* and *treeVariables.h* are used, where the second one serves as a global source of variables, which can be found in the *ROOT* file. At the end of the loop the *ROOT* file is moved to the created folder.

When the analysis of new runs is done, all run level *ROOT* files are merged to a global *ROOT* file called *triggerInfo.root*, which is used as a source for a global analysis, which is executed in a macro *makeGlobalHisto.C*. Results of this macro are plots of different variables dependent on a run number, which are printed in pdf files. At the end of the macro another macro *makePeriodHisto.C* is initialized in a loop over periods and makes similar plots, but delimited on the specific period runs only.

Macros *makeTable.C* and *makeExcel.pl* serve for a period luminosity and trigger summary. The first one loads the global *ROOT* file, sums luminosity and L2A triggers through runs of one period for each period and stores it to text files. Similar text files are also produced for the luminosity and the triggers for each run. These text files are used as a source files for the second

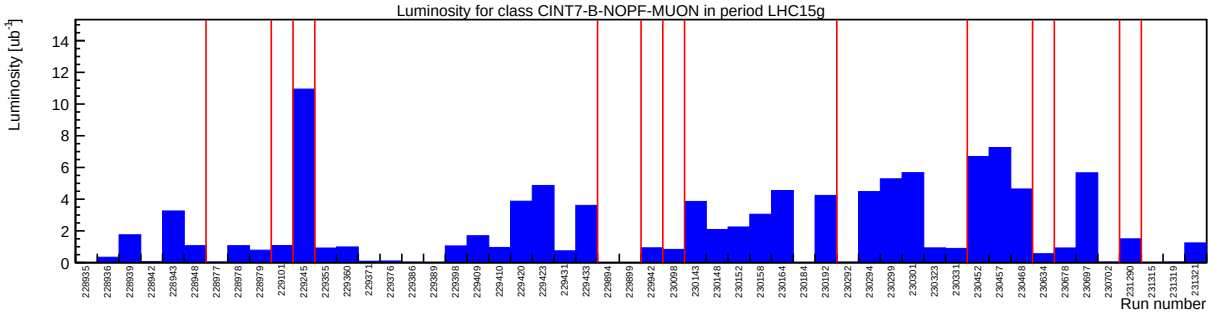

Figure 5.2: A luminosity of a specific class per run in a period LHC15g. Red lines wrap runs obtained from the same LHC fill.

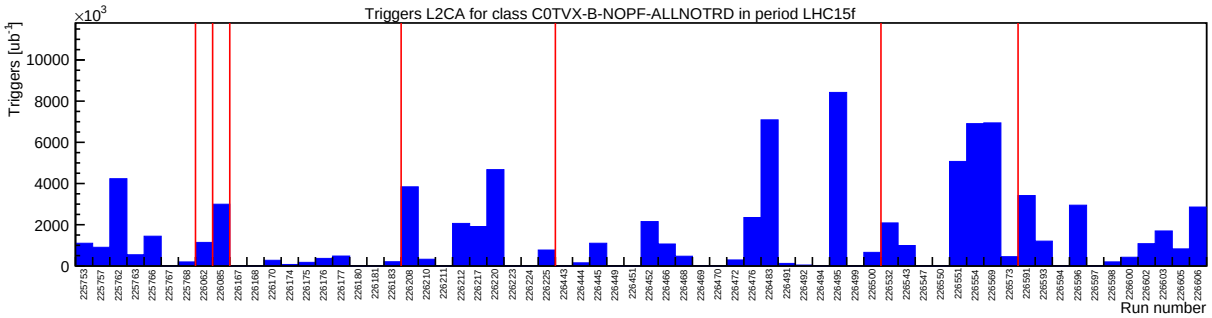

Figure 5.3: Triggers L2A per run in a period LHC15f. Red lines wrap runs obtained from the same LHC fill.

macro, written in perl language [16]. Its only purpose is to transform the text files to one xls file *triggerInfoTable.xls* in a form of excel tables.

5.4 Results

One of the most important results is the aumatization of the whole process. The cronjobs, which trigger a script at a specific time, were used for this purpose. In our case, we use 2 shell scripts. The first one called *newruncheck* starts the program, which performs the analyse. The second one called *croncopy* copies the whole folder with the program and its results to my personal web page [17], where results are available for an external usage. We should also mention, that this is just a temporary solution and in future we would like to provide luminosity and collected statistics class-by-class and run-by-run in OADB and Monalisa.

As mentioned before, the main task is to calculate luminosity for each class and provide these results in various formats. An example of a graphical output is shown in Fig. 5.2. On this plot one can see a calculated luminosity for a class CINT7-B-NOPF-MUON for runs from the LHC15g period only. Our framework provides these plots for every class per every LHC period.

Another important information is the number of collected triggers per class extracted from L2A counts. A nice example can be seen in Fig. 5.3, where class C0TVX-B-NOPF-ALLNOTRD serves as a demonstration. Again, such plots are made for all classes and all periods.

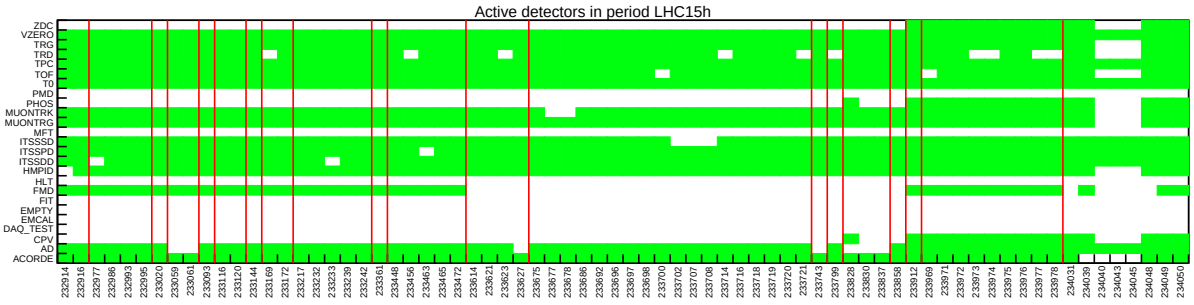

Figure 5.4: A list of active detectors per run in a period LHC15h. Red lines wrap runs obtained from the same LHC fill.

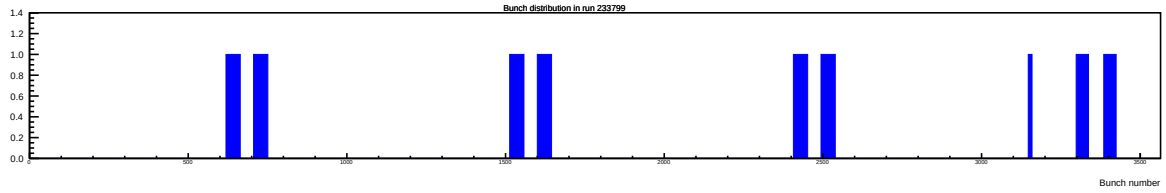

Figure 5.5: An example of a run level analyse. A bunch distribution for the run 233799.

List of ALICE Trigger Codes — Version no. 31_7_2015

Luminosity [ub^-1] per run (for each class)

Run	mu	Bunches	Start_date	Start_time	Run_duration	Period	CTRUE-B-NOPF-ALLNOTRD	C0TVX-B-NOPF-ALLNOTRD	CINT5-B-NOPF-ALLNOTRD
225753	0,0217032	6	2015-06-07	21:42:12	4559	LHC15f	0,03	28,44	28,44
225757	0,0224442	6	2015-06-07	23:02:32	3663	LHC15f	0,02	23,37	23,37
225762	0,022902	6	2015-06-08	00:08:45	6691	LHC15f	0,05	54,84	45,64
225763	0,0218501	6	2015-06-08	02:04:27	962	LHC15f	0,01	7,01	5,88
225766	0,0227351	6	2015-06-08	02:28:08	2284	LHC15f	0,02	18,67	15,55
225767	0,0236907	6	2015-06-08	03:10:58	8	LHC15f	0	0	0
225768	0,0240617	6	2015-06-08	03:14:48	386	LHC15f	0	2,51	2,1
226062	0,000953197	15	2015-06-10	00:27:32	5928	LHC15f	0,01	14,64	14,61
226085	0,00243139	15	2015-06-10	05:43:07	7707	LHC15f	0,01	38,47	38,47
226167	0,00447607	15	2015-06-10	22:08:25	122	LHC15f	0	0	0
226168	0,00450087	15	2015-06-10	22:15:21	131	LHC15f	0	0	0
226170	0,00438547	15	2015-06-10	22:24:46	639	LHC15f	0	3,51	3,51
226174	0,00475168	15	2015-06-10	22:46:54	232	LHC15f	0	0,91	0,91
226175	0,0044179	15	2015-06-10	22:58:01	403	LHC15f	0	2,23	2,23
226176	0,00484228	15	2015-06-10	23:09:54	1485	LHC15f	0	9,38	0
226177	0,0110955	15	2015-06-10	23:39:37	1592	LHC15f	0	12,35	0
226180	0,0107484	15	2015-06-11	00:25:23	10	LHC15f	0	0	0
226181	0,0132279	15	2015-06-11	00:31:40	7	LHC15f	0	0	0
226183	0,0109334	15	2015-06-11	00:36:50	720	LHC15f	0	5,23	0
226208	0,0114322	15	2015-06-11	05:05:31	12551	LHC15f	0,02	98,84	0
226210	0,0112023	15	2015-06-11	08:47:40	1079	LHC15f	0	8,35	0
226211	0,0117202	15	2015-06-11	09:11:24	9	LHC15f	0	0	0
226212	0,0116086	15	2015-06-11	09:18:06	6711	LHC15f	0,01	53,11	0
226217	0,0112205	15	2015-06-11	11:15:33	6369	LHC15f	0,01	49,23	0
226220	0,0115657	15	2015-06-11	13:08:43	7706	LHC15f	0,01	60,32	60,32
226223	0,0113416	15	2015-06-11	15:32:16	11	LHC15f	0	0	0
226224	0,0134721	15	2015-06-11	15:44:46	8	LHC15f	0	0	0
226225	0,0114779	15	2015-06-11	15:51:26	1332	LHC15f	0	9,94	9,94
226443	0,0116601	11	2015-06-12	22:25:01	7	LHC15f	0	0	0
226444	0,0112453	11	2015-06-12	22:32:32	382	LHC15f	0	1,94	1,94
226445	0,0122066	11	2015-06-12	22:45:04	1883	LHC15f	0	14,19	14,19
226449	0,0126376	11	2015-06-12	23:30:07	6	LHC15f	0	0	0
226451	0,0119481	11	2015-06-12	23:36:10	7	LHC15f	0	0	0
226452	0,0130134	11	2015-06-12	23:41:28	3627	LHC15f	0,01	27,76	27,76
226466	0,0121064	11	2015-06-13	00:53:24	1830	LHC15f	0	13,72	13,72
226468	0,012815	11	2015-06-13	01:36:42	807	LHC15f	0	6,07	6,07
226469	0,0134082	11	2015-06-13	01:55:26	21	LHC15f	0	0,13	0,13
226470	0,0131488	11	2015-06-13	02:00:49	10	LHC15f	0	0	0
226472	0,0126281	11	2015-06-13	02:06:23	768	LHC15f	0	3,73	3,73
226476	0,0126357	11	2015-06-13	02:34:18	3954	LHC15f	0,01	30,32	30,32
226483	0,0126672	11	2015-06-13	03:48:24	11944	LHC15f	0,02	91,49	91,49
226491	0,0127673	11	2015-06-13	07:11:41	210	LHC15f	0	1,57	1,57
226492	0,0125613	11	2015-06-13	07:19:42	79	LHC15f	0	0,56	0,56

Figure 5.6: An example of summary statistics in an excel table. A luminosity of each class per run with additional informations.

The last but not least product of global statistics are plots of miscellaneous variables and their dependencies on the run number. Fig. 5.4 serves as an instance of this statistics. Green fields represent ALICE subdetectors, which were on during a specific run. The program makes these plots for every LHC period.

Not only global statistics are made, but also a run level informations are obtained and stored in a form of histograms. An example bunch crossing distribution is shown in Fig. 5.5, which is created for every run. Many other plots can be made on request.

A run/trigger coordinators will appreciate the last important result of this program - a summary of luminosities and triggers for each class per run or per LHC period organized in well-arranged excel tables. A snapshot of this file is shown in Fig. 5.6 and original file can be found on the mentioned webpage under the name *triggerInfoTable.xls*. As the file is periodically updated, the coordinators have a fresh informations on the collected statistics.

Chapter 6

Summary

Small-x physics is an interesting object of studies. A lot of work has been done by H1 and ZEUS Collaborations from data obtained at HERA [2]. Although the LHC facility wasn't primary built to continue in this studies, ultra-peripheral collisions give an opportunity to do so. The rapidity dependence of the cross section at LHC energies has been measured [1]. A calculation of the dependence of the cross section on transferred momentum t is in progress now and this report states current results.

First, we had to understand given data and pick the right selection criteria. An impact of these cuts on original data are in Tabs. 3.1, 3.2 and 3.3. Plots of mass, p_t and p_t^2 distributions can be found in Figs. 3.1-3.6.

Important part of adjusting the measured data for correct cross section computation is to examine the process with simulated Monte Carlo data. Influence of the ALICE detector performance is introduced in Sec. 3.2.2 and result is presented in Fig. 4.1. Because we deal with a small number of measured data, we had to also think out the best binning order. This is described in Sec.3.2.3 and resulting plots are in Figs. 4.2 and 4.3.

The last thing we have achieved were fits of the Monte Carlo coherent data. We used two different approaches. Using a form factor deduced from the QCD with fixed range of Yukawa potential $a = 0.7$, we came up with a value of 6.09 ± 0.23 fm. Another approach was to use as a form factor a Gaussian function. As a result we got the transversal nuclear size 4.5 ± 1.3 fm. More details in Sec. 4.3 and Figs. 4.4-4.7.

Currently, we have analysed the coherent part of the Monte Carlo data. The next step is to mix coherent and incoherent samples in order to come closer to the measured data. Also an investigation of effects of a reaction $\gamma\gamma \to \mu\mu$ has to be done in order to separate out unwanted background. Once this will be done, we can apply our conclusions on measured data, fit them and compute the cross section.

We have also developed the luminosity computation framework, which can daily automatically update informations on luminosity collected at ALICE detector classes. Results are accessible to the whole collaboration and serves well to the run/trigger coordinators. This was done under the supervision of ALICE trigger coordinator Evgeny Kryshen.

Bibliography

[1] E. Abbas *et al.* [ALICE Collaboration], "Charmonium and e^+e^- pair photoproduction at mid-rapidity in ultra-peripheral Pb-Pb collisions at $\sqrt{s_{\rm NN}}$=2.76 TeV," Eur. Phys. J. C **73** (2013) 11, 2617 [arXiv:1305.1467 [nucl-ex]].

[2] H. Abramowicz *et al.* [H1 and ZEUS Collaborations], arXiv:1506.06042 [hep-ex].

[3] MCLERRAN, L.:The CGC and the Glasma: Two Lectures at the Yukawa Institute. Physics Department and Riken Brookhaven Center, Brookhaven National Laboratory, 2010.

[4] S. A. Kulagin and R. Petti, Phys. Rev. C **82** (2010) 054614 [arXiv:1004.3062 [hep-ph]].

[5] A. J. Baltz, G. Baur, D. d'Enterria, L. Frankfurt, F. Gelis, V. Guzey, K. Hencken and Y. Kharlov *et al.*, "The Physics of Ultraperipheral Collisions at the LHC," Phys. Rept. **458** (2008) 1 [arXiv:0706.3356 [nucl-ex]].

[6] C. A. Bertulani, S. R. Klein and J. Nystrand, Ann. Rev. Nucl. Part. Sci. **55** (2005) 271 [nucl-ex/0502005].

[7] A. Adeluyi and C. Bertulani, Phys. Rev. C **84** (2011) 024916 [arXiv:1104.4287 [nucl-th]].

[8] J. G. Contreras and J. D. Tapia Takaki, Int. J. Mod. Phys. A **30** (2015) 08, 1542012.

[9] K. A. Olive *et al.* [Particle Data Group Collaboration], Chin. Phys. C **38** (2014) 090001.

[10] R. Vogt, "Ultrarelativistic heavy-ion collisions," Elsevier, (2007).

[11] G. Usai, "Why measuring lepton pairs," [`http://gruppo3.ca.infn.it/usai/?Research:Physics_highlights:Why_measuring_lepton_pairs` cited on 26.6.2015].

[12] K. Aamodt *et al.* [ALICE Collaboration], "The ALICE experiment at the CERN LHC," JINST **3** (2008) S08002.

[13] S. Klein and J. Nystrand, Phys. Rev. C **60** (1999) 014903 [hep-ph/9902259].

[14] E. Kryshen *et al.*, "ALICE trigger group internal notes."

[15] I. Antcheva *et al.*, "ROOT: A C++ framework for petabyte data storage, statistical analysis and visualization," Comput. Phys. Commun. **180** (2009) 2499 [arXiv:1508.07749 [physics.data-an]].

[16] J. Allen, "Perl programming language, Manual pages," [`http://perldoc.perl.org/perl.html` cited on 1.9.2015].

[17] R. Lavicka, "Personal web pages," [`https://rolavick.web.cern.ch/rolavick/` cited on 1.9.2015].